Frequency-Based Response of Damped Outrigger Systems for Tall Buildings

by

Renard Gamaliel

B.S., Civil and Environmental Engineering (2007)
University of California at Berkeley

Submitted to the Department of Civil and Environmental Engineering
in Partial Fulfillment of the Requirements for the Degree of
Master of Engineering in Civil and Environmental Engineering

at the

Massachusetts Institute of Technology
June 2008

Signature of Author _____
Department of Civil and Environmental Engineering
May 19, 2008

Certified by _____
Jerome J. Connor
Professor of Civil and Environmental Engineering
Thesis Supervisor

Accepted by _____
Daniele Veneziano
Chairman, Departmental Committee for Graduate Students

Frequency-Based Response of Damped Outrigger Systems for Tall Buildings

by

Renard Gamaliel

Submitted to the Department of Civil and Environmental Engineering
on May 19, 2008 in Partial Fulfillment of the
Requirements for the Degree of Master of Engineering in
Civil and Environmental Engineering

ABSTRACT

The outrigger structural system for tall buildings is known to be effective in reducing lateral drift under quasi-static wind loading. Although keeping lateral deflection below the required value is certainly important, it is found that in most tall buildings without supplementary damping, the design for stiffness is usually governed by occupant comfort under lateral acceleration.

This thesis describes the concept of incorporating fluid viscous dampers in the outrigger system to add supplementary damping into the structure. A 40-story building installed with the variant outrigger system is analyzed for dynamic response due to wind effects such as buffeting and vortex shedding. By constructing an 80-dof discrete lumped mass model, and using a frequency-based response approach, two configurations of dampers, namely series and parallel damping are studied in detail. The effect of increasing damper size to overall achievable building damping is monitored for both configurations. Additionally, design and constructability issues with regards to the implementation of the systems are discussed.

Thesis Supervisor: Jerome J. Connor
Title: Professor of Civil and Environmental Engineering

ACKNOWLEDGEMENTS

First of all, I would like to thank my parents for giving me the opportunity to pursue this degree at MIT. I truly appreciate your efforts in making my education experience the best ever possible. To my brother, who has been a mentor throughout my education life, for all your help and advice, I deeply thank you.

To Professor J. J. Connor, who served as my advisor in this thesis, I would like to thank you for sharing your vast amount of knowledge and experience in the many discussions we had. Your support and guidance have made the completion of this thesis possible.

Not forgetting my fellow M. Eng. HPS friends, who have contributed to my diverse learning, and have provided me with encouragement and mental support throughout writing this thesis, I thank you all. It has been a pleasure working together with all of you during the past 9 months.

Table of Contents

List of Figures

List of Tables

CHAPTER 1: INTRODUCTION

In recent years, taller and more slender buildings are being built across the globe with the intention of maximizing rentable space and as means of creating a signature structure in the heart of a city. Advancement in structural engineering, together with improvements in fabrication and construction techniques, has continued to sustain this demand of achieving greater heights. Load tends to accumulate rapidly in high-rise structures, and in order to minimize the size of members, high strength materials have been more commonly utilized. While fabricators are able to work with higher yield strength steel, the Young's Modulus has remained constant. Material advancement of this nature has contributed to a recent shift in design methodology from strength-based to motion-based design. Furthermore, particularly for slender buildings, the dynamic resonant response of the structure to incident wind gusts and vortex shedding leads to significant motion problems. Structural engineers are continuously being challenged to provide innovative, efficient structural schemes that control both drift and acceleration of the building in order to satisfy serviceability constraints as well as human comfort levels. The savings in steel tonnage and cost can be significant in high-rise buildings if certain techniques are employed to utilize the full capacities of the structural elements.

The outrigger system has been proven to be a highly effective way of satisfying the motion constraints of tall and slender buildings. The behavior of the outrigger system under quasi-static wind loading is well understood and has been studied extensively. However, under dynamic wind loading, the response of the outrigger system cannot be predicted with a high level of accuracy. A number of factors govern the dynamic response of tall buildings which include shape, stiffness, mass and damping. While the effect of shape can be assessed by wind

tunnel testing, and the mass and stiffness can be computed with reasonably accuracy by the structural engineer, tall buildings have low intrinsic damping which is difficult to quantify other than through experimentation. This thesis will explore the incorporation of supplementary damping in the outrigger system, which aims to remove the dependability of the structure to low, variable intrinsic damping.

1.1 Outrigger Structural System

For medium high-rise structures, the traditional approach to lateral support is to provide trussed bracing at the core and around stair wells. Additional lateral resistance is provided by moment-connected frames at any other convenient plan location. Due to the need of creating open space, building designers have been locating lateral systems primarily in the core. Hence, the core is solely responsible in providing the lateral stiffness. However, when buildings are taller than 500 ft (150 m) or so, the braced core system alone does not have enough stiffness to keep wind drift down to acceptable limits.

The technique of using outriggers on a braced core with exterior columns has evolved over the past few decades. This system removes the uncoupling of the core from the perimeter column, enabling buildings to utilize its total width when resisting lateral loads. A typical outrigger system on a braced core is shown in Figure 1. When the building is subjected to lateral forces, tie-down action of the outrigger restrains the bending of the core by introducing a point of inflection in the deflection profile. The reversal in curvature reduces the lateral motion at the top. In many cases, outriggers are also used around the perimeter to engage the columns that are not connected to the main outrigger trusses. This is what is referred to as a belt truss system, often used together with the main outriggers. The outrigger and belt truss system is capable in providing up to 25 to 30 percent additional stiffness in contrast to a system

without such trusses (Taranath, 1988). The main reason attributes to the fact that the façade columns now participate in lateral load resistance.

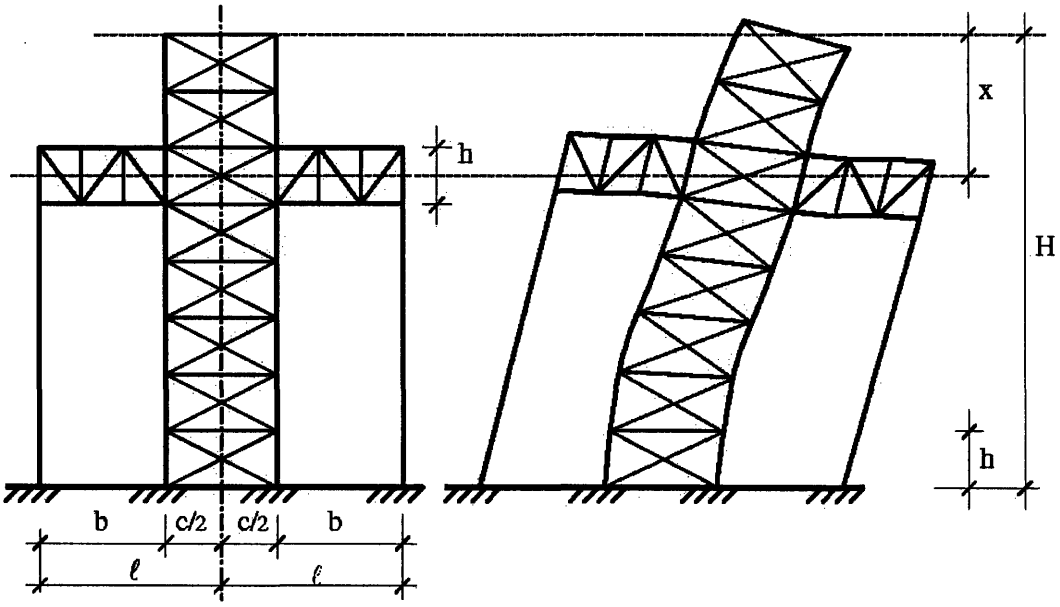

Figure 1: Typical outrigger sytem on braced core (Hoenderkamp, 2003)

Some benefits as outlined by The Council of Tall Buildings and Urban Habitat are immediately realized through the use of outriggers. Besides the reduction of core moment at the outrigger intersection, the system equalizes the differential shortening of exterior columns resulting from temperature and axial load imbalance. Another effect of using outriggers is the significant reduction of net tension and uplift force at the foundation level. The placement of the outrigger arm can easily be meshed with aesthetic and functional considerations. For example, the outrigger system can be incorporated at the mechanical floor, which will otherwise be unusable space. From an economic point of view, the outrigger system will eliminate the need for moment-connected frames at the façade, i.e. the exterior framing can consist of simple beam-column shear connections.

Other than the benefits, one should realize that the outrigger system does not add shear rigidity to the structure; therefore, the core must be designed to carry all the shear force. Also, creating an infinitely rigid link is virtually impossible in the real world, and the outrigger arm may take up more than one floor in the building. Certain design considerations such as the outrigger-core connection design will be examined in more detail in the later part of this thesis.

1.2 Passive Damping in High-Rise Buildings

Traditionally, the design approach to control dynamic wind-induced response is to increase stiffness and strength of the lateral load resisting system. By increasing stiffness, the natural period of the building is reduced, which generally leads to a reduction in dynamic response. Providing stiffness to a building comes with significant cost and leads to larger member sizes, hence reducing the building's effective area. Furthermore, for seismic excitation, which has relatively short periods, increased stiffness may cause the building to more likely respond in resonance with the ground motion. As such, solutions involving damping are often preferred in mitigating the dynamic response of tall buildings.

Damping is defined as the process by which physical systems such as structures dissipate and absorb energy input from external excitations (Connor, 2003). There are two main class of damping systems, namely passive versus active damping. Passive dampers by definition have fixed properties and do not require external source of energy. A passive damping system cannot be modified readily once installed; therefore a more conservative design estimate is required to account for unexpected loading conditions. An active type damper typically utilizes an actuator and sophisticated monitoring system to adjust the system properties according to the physical loading condition at real time. Since an external energy source such as electricity is required for the actuator to function, the reliability of active damper systems can be

questionable especially during an extreme loading situation. Often the case, designing for a passive damping system is preferred for its simplicity, reliability and its lower cost compared to active damping systems.

When the predicted building motion exceeds human comfort levels, the most common method to mitigate the motion problem is to install a tuned mass damper (TMD) or a tuned liquid damper (TLD) at the top of the building. A tuned mass/liquid damper system can often be designed to provide 2-4% critical damping, which means that the resonant response can be reduced by a factor of two (Smith & Willford, 2007). Inertia-based dampers such as the TMD and TLD are not always the best solution due to the following reasons:

- These devices are large, heavy, and occupy a lot of space at the top of the building
- They only work for a particular frequency of excitation in which they are tuned at, i.e. if there are several modes of concern, several sets of such devices tuned at different frequencies are required
- The natural period of the building may change over time and with response amplitude, therefore the device may become less effective over time
- Usually, only one large damper unit is provided to save space and cost, this raises issues with reliability should the unit or one component of it were to fail
- TMD's are not effective against severe seismic events with a wide range of frequencies lasting over a short duration

Another way of providing damping in high-rise buildings is to install resistance devices such as fluid viscous dampers, visco-elastic dampers, and friction dampers. These devices operate based on the relative motion between the two points in which they are attached. It is desirable to locate the damper in a location connecting two points having significant relative

displacements when subjected to the particular excitation of concern. One of the main advantages of these devices is that they do not need frequency tuning. Although there is always an optimum resistance setting for a given application, the overall damping achieved is usually not very sensitive to the exact properties of the device itself.

This thesis will explore the use of fluid viscous dampers as a mechanism of passive damping. Viscous dampers are piston-type devices with arrangements of seals and orifices which generates a resistance force as fluid is passed through it. The damper force generated is a function of the velocity between the two ends of the device, and is given by

$$F_{damper} = c\dot{u} \tag{1.1}$$

where c represent the damping coefficient in N.s/m and

$\dot{u}$ is the velocity, i.e. the time derivative of displacement

The objective of using viscous dampers is to reduce building deflections, but will this increase the loads in the building columns? In fact, the force generated from damping is completely out of phase with stresses due to flexing of the columns, thus reducing the column stresses instead. Unlike other types of damping such as yielding elements, friction devices, plastic hinges, and visco-elastic elastomers, fluid viscous dampers vary their outputs with stroking velocity. Consider an example of a building with viscous dampers mounted in the diagonal bracings. During a seismic event, the columns reach its maximum stress when the building has displaced a maximum amount from its original position. At this point, the velocity is zero; therefore no force is generated in the viscous damper. When the building flexes back in the opposite direction, maximum velocity is reached at the point of zero displacement from the original position, meaning the building is upright. At this time, the exact opposite is observed.

The viscous damper is giving out its maximum output while the stresses in the columns due to bending are zero. Figure 2 shows an example of a viscous damper with 50,000 lbs output made by Taylor Devices, Inc. The exact placement and configuration of viscous dampers to be installed in the outrigger system will be discussed in detail in Chapter 5.

Figure 2: Viscous dampers (Taylor Devices, Inc., 2008)

1.3 Thesis Organization

The objective of this thesis is to study the response of damped outrigger systems subjected to dynamic wind-excitation over a range of frequencies. Wind loads usually governs the design of tall buildings (greater than 30 stories), more so than earthquake excitation. In order to accomplish this, a model of a typical slender building is first constructed, using discrete lumped masses. The construction of the discrete system will be explained in Chapter 2. The determination of design forces will be estimated by means of code design standards and qualitative reasoning, as discussed in Chapter 3. To ensure that the model works with reasonable accuracy, the results for the static case will be compared to the analytical solution of a single outrigger. Derivations for the analytical solution will be presented in Chapter 4. All

analysis procedures will be encoded into a MATLAB program to simulate the process efficiently. Chapter 5 will focus on the analysis of damped outrigger systems using a frequency-based approach. Once the structural behavior has been analyzed, issues regarding possible implementation of the damped outrigger system will be discussed in Chapter 6, particularly with regards to design and construction aspects. The next section will describe the building parameters that will be used throughout the analysis process.

1.4 Building Parameters

To represent a tall slender building, a 40 story rectangular high-rise structure with a base dimension of 30 m by 30 m will be analyzed. The floor-to-floor height is 4 m contributing to a total building height of 160 m, and an aspect ratio (H/B) of 5.33. The building will have a 14 m by 14 m central concrete core with a thickness of 40 cm. Consequently, the outrigger links are 8 m in length, spanning from the core to the perimeter columns. It is assumed that the floor system will be a 15 cm concrete slab on metal decking. The building will have two outrigger arms cantilevering from the core to the perimeter columns from each of the side of the core. As a result of the geometry, 4 perimeter columns will participate in lateral force resistance in each of the principal directions. W14x398 sections with an approximate cross-section area of 0.15 m^2 will be utilized as the perimeter columns. The properties of concrete and steel used are as follows:

- Concrete Modulus of Elasticity, $E_c = 2.482 \times 10^{10}\ Pa$
- Concrete Density, $\rho_c = 2400\ kg/m^3$
- Steel Modulus of Elasticity, $E_s = 2 \times 10^{11}\ Pa$

Figure 3 summarizes the building dimensions described.

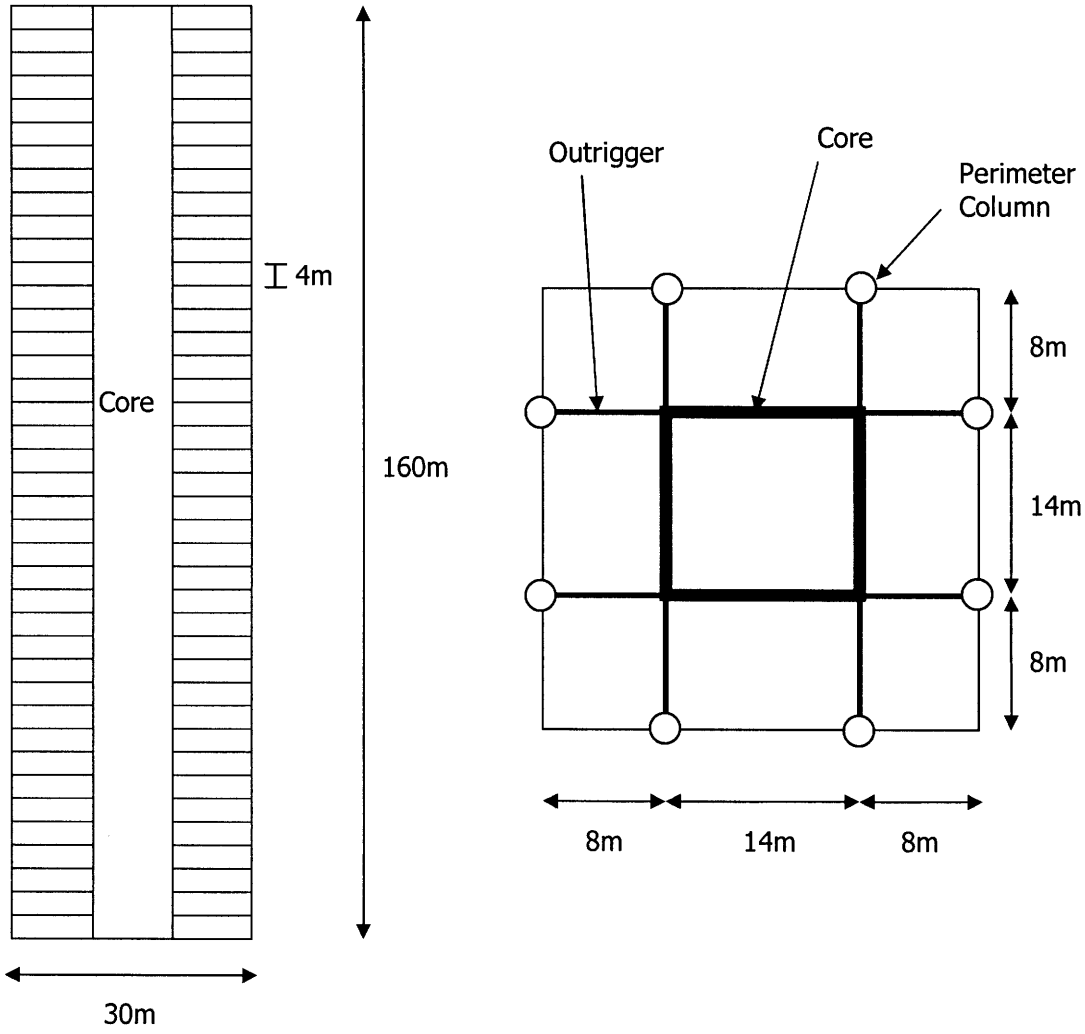

Figure 3: Buildings dimensions in elevation (left) and plan (right)

CHAPTER 2: DISCRETE MODEL

2.1 Level of Abstraction

The art of modeling a structural system for dynamic loads relates to a process by which one abstracts the essential properties of an actual physical system into an idealized mathematical model. In this thesis, a heuristic approach based on physical approximations will be employed.

To create a realistic model of the proposed building described in Chapter 1, each floor of the building will be discretized as a series of masses lumped at the center of the core. Each mass will have two degrees of freedom namely 1 translational degree of freedom in the horizontal direction and 1 rotational degree of freedom. It is reasonable to define the active degrees of freedom at each floor because loads from the façade are transferred to the core through the floor diaphragm. Therefore, external loads can be lumped using the concept of tributary areas, and applied at each node level. Due to negligible deformation in the vertical direction, the vertical translation degree of freedom has been neglected to simplify the model.

Figure 4 shows a similar discrete lumped mass model for a 5 story building to illustrate the basic concept; where u is the horizontal displacement, θ is the rotation, P is the applied load, and m is the nodal mass. Following this concept, the actual 40 story model will have 40 lumped masses, 40 nodal translation degrees of freedom, and 40 nodal rotational degrees of freedom. The stiffness and mass matrix will be determined next in order to solve the general discrete equation of motion written in matrix form as

$$\boldsymbol{M\ddot{U} + C\dot{U} + KU = P} \tag{2.1}$$

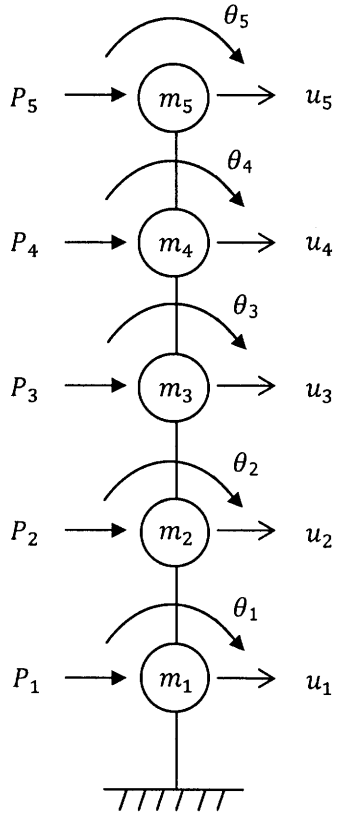

Figure 4: Discrete lumped mass model for a 5 story building

2.2 Determination of Stiffness Matrix

To obtain the global stiffness matrix, the direct stiffness approach is used. Since there are a total of 80 active degrees of freedom representing 40 floors, the dimension of the global stiffness matrix $\boldsymbol{K}$ is 80 by 80. The K matrix follows the basic form as follows,

$$\begin{bmatrix} k1_{BB}+k1_{AA} & k1_{AB} & & & & & 0 & \\ k1_{BA} & k1_{BB}+k2_{AA} & k2_{AB} & & & & & \\ & k2_{BA} & k2_{BB}+k3_{AA} & & & & & \\ & & & & \ddots & k38_{AB} & & \\ 0 & & & & k38_{BA} & k38_{BB}+k39_{AA} & k39_{AB} & \\ & & & & & k39_{BA} & k39_{BB}+k40_{AA} & \end{bmatrix} \begin{bmatrix} u_1 \\ \theta_1 \\ u_2 \\ \vdots \\ u_{40} \\ \theta_{40} \end{bmatrix}$$

The member stiffness matrices are given by

$$k(n)_{AA} = \begin{bmatrix} \left(\frac{AE}{L}sin^2a + \frac{12EI}{L^3}cos^2a\right) & \frac{6EI}{L^2}cos\,a \\ \frac{6EI}{L^2}cos\,a & \frac{4EI}{L} \end{bmatrix}$$

$$k(n)_{AB} = \begin{bmatrix} \left(-\frac{AE}{L}sin^2a + \frac{12EI}{L^3}cos^2a\right) & \frac{6EI}{L^2}cos\,a \\ -\frac{6EI}{L^2}cos\,a & \frac{2EI}{L} \end{bmatrix}$$

$$k(n)_{BA} = \begin{bmatrix} \left(-\frac{AE}{L}sin^2a + \frac{12EI}{L^3}cos^2a\right) & -\frac{6EI}{L^2}cos\,a \\ \frac{6EI}{L^2}cos\,a & \frac{2EI}{L} \end{bmatrix}$$

$$k(n)_{BB} = \begin{bmatrix} \left(\frac{AE}{L}sin^2a + \frac{12EI}{L^3}cos^2a\right) & -\frac{6EI}{L^2}cos\,a \\ -\frac{6EI}{L^2}cos\,a & \frac{4EI}{L} \end{bmatrix}$$

where,

A = area of the core

E = elastic modulus of the core

I = moment of inertia of the core with respect to the bending axis

L = floor height, and

a = angle of reference with respect to the global coordinate

2.3 Determination of Mass Matrix

The mass matrix M is a diagonal matrix containing the floor mass as well as the rotational inertia of the following form,

$$M = \begin{bmatrix} M_1 & & & & & & 0 \\ & J_1 & & & & & \\ & & M_2 & & & & \\ & & & J_2 & & & \\ & & & & \ddots & & \\ & & & & & M_{40} & \\ 0 & & & & & & J_{40} \end{bmatrix}$$

Since the floor layout is the same throughout the building height, $M_1 = M_2 = \cdots = M_{40} = M$. The quantity M is obtained from the mass of the concrete floor slab and the mass of the concrete core with a tributary length of 1 floor, i.e. halfway up to the floor above and halfway down to the floor below. Similarly, the rotational inertia entries are equal throughout the height, thus $J_1 = J_2 = \cdots = J_{40} = J$. Rotational inertia is assumed to be provided by the concrete core only, and the floor slabs have negligible effect on rotation because it is not rigidly attached to the core. Calculations for core moment of inertia, nodal mass and nodal rotational inertia can be found in Appendix A.

CHAPTER 3: WIND EFFECTS

3.1 Characteristics of Wind

3.1.1 Introduction

Wind is a phenomenon of great complexity due to the many situations that arise from its interaction with structures. In wind engineering, simplifications are made to arrive at meaningful predictions of wind behavior by characterizing their flow states into the following distinguished features:

- Variation of wind velocity with height
- Turbulent nature of wind
- Probabilistic approach
- Vortex shedding phenomenon
- Dynamic nature of wind structure interaction

Each of these features will be described briefly.

3.1.2 Variation of Wind Velocity with Height

As fluids move across a solid surface, viscosity causes shear forces to be generated in the direction opposite to the moving fluid. This effect occurs between the atmosphere and the surface of the Earth. The velocity of the air directly adjacent to the Earth's surface is zero. A retarding effect occurs in the layers near the ground, which in turn slows down the outer layers successively. As distance from the ground increases, the retarding effect gradually decreases and becomes negligible. Figure 5 shows the variation of wind velocity with height.

As seen in Figure 5, the wind profile takes on an asymptotic parabolic shape. The height at which the velocity stops increasing further is called the gradient height, and the corresponding velocity is referred to as the gradient velocity. The shape and size of the curve is dependent on a number of factors, mainly the viscosity of the air, and the random eddying motions in the wind which relates to the terrain over which the wind is blowing.

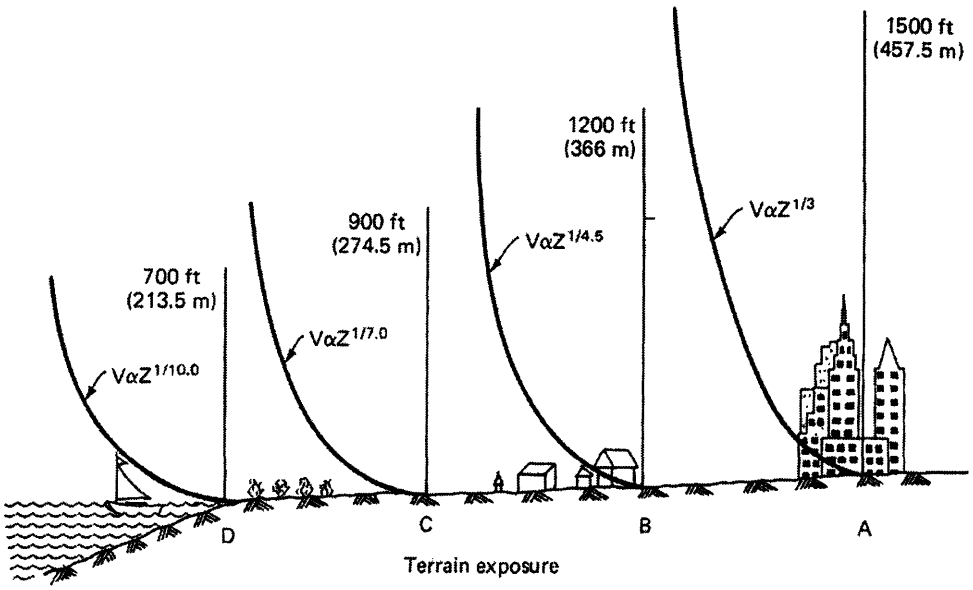

Figure 5: Variation of wind velocity with height (Taranath, 1988)

In engineering practice, wind profile in the atmospheric layer is well represented by the power law expression of the form:

$$V_Z = V_g \left(\frac{Z}{Z_g}\right)^{\alpha} \tag{3.1}$$

Where V_Z = the mean wind speed at height Z above the ground surface

V_g = gradient wind speed assumed constant above the boundary layer

Z = the height above the ground

Z_g = depth of boundary layer

α = power law coefficient

This characteristic of wind velocity variation with height is fairly well understood and has been incorporated in most building codes.

3.1.3 Turbulent Nature of Wind

Superimposed on the mean wind speed is the turbulence or gustiness of wind, which produces deviations in the wind speed above and below the mean, depending whether there is a gust or lull in the wind action. The average or mean wind speed used in many building codes of the United States is the fastest-mile-wind, which can be thought of as a maximum velocity measured over the one mile of wind passing through an anemometer. Generally, the wind speed used for structural design ranges from 60-120 mph (27-54 m/s) giving an averaging period of 30-60 seconds, hence the loading is considered quasi-static.

The motion of wind is generally turbulent because air has a low viscosity of about one sixteenth of water. Flow of air near the earth's surface constantly changes in speed and direction due to the obstacles that causes disruptions to the main direction of flow. Turbulence that is generated creates gusts that have a wide range of frequencies and amplitude. Tall buildings are sensitive to gusts that last about 3-4 seconds. Therefore, it is important that one uses the gust speed rather than the mean wind speed in the determination of wind load.

3.1.4 Probabilistic Approach to Wind Load Determination

In engineering science, the intensity of an event is defined as a function of the frequency of recurrence or more commonly referred to as return period. Similarly in wind engineering, the speed of wind is considered to vary with duration and return period. For example, the fastest-mile wind 33 ft (10 m) above the ground in Dallas, Texas, corresponding to a 50-year return period is 67 mph (30 m/s) as compared to the value of 71 mph (32 m/s) for a 100-year recurrence interval. A return period of 50 years corresponds to a probability of occurrence of 1/50 = 0.02 = 2 percent. This means that the chance of a wind exceeding 67 mph will occur in Dallas within a given year is 2 percent.

Now, suppose that a building with a lifetime of 100 years is to be designed using a wind speed of 67 mph. We are interested to calculate the probability that the design wind will be exceeded during the lifetime of the structure. The probability that this wind speed will not be exceeded in any year is 49/50. However, the probability of the wind speed not being exceeded consecutively over 100 years is $(49/50)^{100}$. Therefore, the probability that this wind speed will be exceeded at least once in 100 years is $1 - (49/50)^{100} = 0.87 = 87$ percent. This clearly shows that even though the 50 year wind has a very low probably of being exceeded at any given year, a high probability of it being exceeded over the lifetime of the structure exists. In actual structures however, the probability of the structure being overstressed is much lower because of the built-in safety factors taken into account in the design process.

3.1.5 Vortex Shedding

In general, wind blowing past a body can be diverted into three mutually perpendicular directions, giving rise to forces and moments in the three directions. In structural engineering, the force and moment corresponding to the vertical axis are of little significance. The flow of wind can be considered to be two dimensional. Figure 6 shows a simplified diagram of wind flow in two dimensions. Along wind contributes to drag forces and the transverse wind is often referred to as cross wind. The along wind predominantly imposes a quasi-static pressure on the building surface with some fluctuations due gust effects as discussed in Section 3.1.3. In the cross wind direction, dynamic forces are generated due to the formation of wake vortices as wind flows around the building. For tall buildings, the cross wind response dominates over the along wind response. This may be counter intuitive, as is the case for the complex nature of turbulence and wake formation.

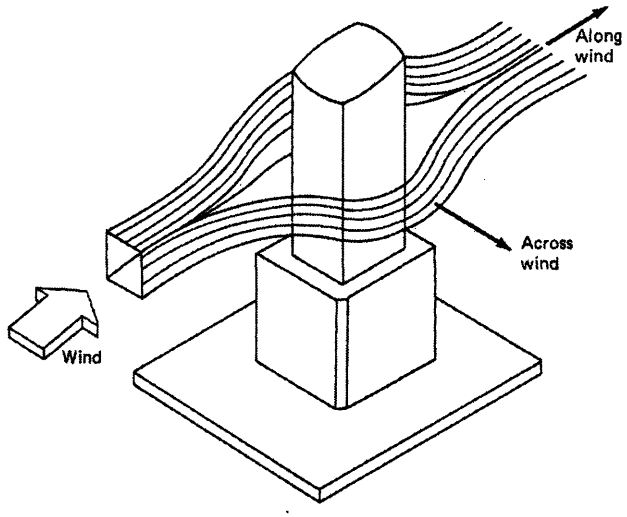

Figure 6: Simplified two dimensional flow of wind (Taranath, 1988)

To understand the nature of these wake formations, consider a cylindrical shaped building subjected to a smooth wind flow. At first, parallel streamlines are displaced on either side of the cylinder, and this results in spiral vortices being shed periodically from the sides of the cylinder into the downstream flow of wind called the wake. At low wind speeds, the vortices are shed symmetrically in pairs from each side. The force that the building feels at this instance is an additional drag force in the along wind direction due to shearing action at the side of the building. At higher speeds, the vortices are shed alternately first from one and then from the other side of the cylinder. When this occurs, an impulse in the transverse direction is generated. The alternate shedding of vortices in the transverse direction which gives rise to structural vibrations is called vortex shedding or the Von Karman vortex street. This phenomenon of alternate shedding of vortices is shown in Figure 7.

The frequency of the transverse pulsating forces caused by vortex shedding is given by

$$f = \frac{S_T V}{D} \tag{3.2}$$

Where f = frequency of the vortex shedding in Hertz

V = mean wind speed at the top of the building

S_T = Strouhal number for the shape (a dimensionless parameter)

D = diameter of the building

The Strouhal number varies irregularly with wind velocity up to a limit of 0.21 for a smooth cylinder. This limit is reached for a velocity of about 50 mph (22 m/s) and remains almost constant at 0.20 for wind velocities between 50-115 mph (22-51 m/s).

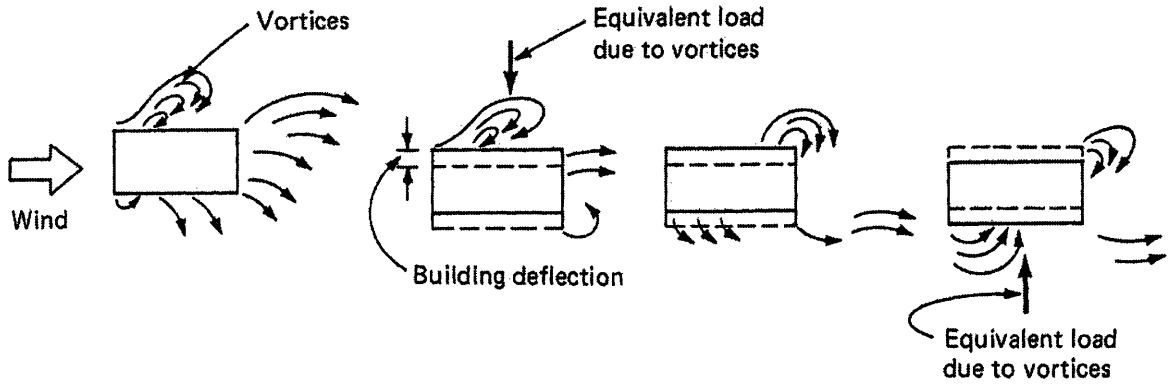

Figure 7: Vortex shedding phenomenon (Taranath, 1988)

3.1.6 Dynamic Nature of Wind

Unlike the mean velocity of wind which can be considered quasi-static due to its long period, wind loads associated with gustiness or turbulence change creates effects larger than if the same loads are applied gradually. A tall, slender building can have a significant dynamic response to wind because of buffeting. The intensity of wind loads depend on how fast it varies and also on the response of the structure. For example, the period of oscillation for a tall steel building in the height range of 200-400 m is between 5 to 10 seconds, whereas, a 10 story concrete masonry building may have a period of 0.5 to 1 second. The gusts can be considered quasi-static if the wind load increases and diminish in a time much longer than the period for the building. For example, a wind gust growing to its strongest pressure and decreasing to zero in 2 seconds is a dynamic load for a tall building with a period of 5 to 10 seconds. However, the same 2 seconds gust is considered a quasi-static load for a low-rise building with a period of less than 2 seconds.

3.2 Determination of Wind Loads

3.2.1 Static Case

For the purpose of analysis in this thesis, ASCE7-05 Minimum Design Loads Provisions will be used. The building is assumed to be located in Boston, MA with exposure category B, i.e. a city environment with closely spaced obstructions. The basic wind speed in this region is 105 mph (47 m/s) as defined by the code. This value is a nominal design 3-second gust wind speed at 33 ft (10 m) above ground for Exposure C category. The formula for the velocity pressure evaluated at height z is given by the following equation:

$$q_z = 0.613 K_Z K_{zt} K_d V^2 I \ (N/m^2) \tag{3.3}$$

Where K_Z = velocity exposure coefficient

K_{zt} = topographic factor

K_d = wind directionality factor

V = basic wind speed, and

I = importance factor

For rigid buildings of all heights, design wind pressures for Main Wind-Force Resisting Systems (MWFRS) shall be determined by the following equation:

$$p = qGC_p - q_i(GC_{pi}) \ (N/m^2) \tag{3.4}$$

Where $q = q_z$ for windward walls evaluated at height z above the ground

$q = q_h$ for leeward walls, side walls, and roofs, evaluated at the mean roof height, h

$q_i = q_h$ for windward walls, side walls, leeward walls, and roofs of enclosed buildings and for negative internal pressure evaluation in partially enclosed buildings

G = gust effect factor

C_p = external pressure coefficient, and

(GC_{pi}) = internal pressure coefficient

Since performing a full blown wind analysis is not the objective of this thesis, the maximum pressure value at the top of the building (z = 160 m) is calculated, and this pressure will be applied at every floor of the building, giving a conservative design force. Calculations are performed for both the windward pressure and the leeward pressure. The addition of these two numbers will give us the combined pressure. Finally, this combined pressure is multiplied by the tributary area corresponding to each nodal point in the discrete model, and the nodal point force for use in static analysis is obtained. Table 1 shows a summary of the parameters used in obtaining the design wind pressures and the equivalent nodal point force of interest. For complete detail, it is best to refer to ASCE7-05 directly.

Table 1: Summary of wind loading parameters

Basic Wind Speed, V	47	m/s
Exposure Category	B	
Importance Factor, I	1.00	
Directionality Factor, K_d	0.85	
Topographic Factor, K_{zt}	1.00	
Gust Factor, G	0.85	
Internal Pressure Coefficient, GC_{pi}	-0.18	
C_p (Windward)	0.8	
C_p (Leeward)	0.5	
Height of building, z	160	m
Mean roof height, h	160	m
Velocity Pressure Coefficient, K_z	1.6	
Velocity Pressure, q_z (windward)	1,842	N/m^2
Velocity Pressure, q_h (leeward)	1,842	N/m^2
Pressure, p (windward)	1,584	N/m^2
Pressure, p (leeward)	1,114	N/m^2
Total Design Pressure	2,698	N/m^2
Tributary Area	120	m^2
Nodal Point Force	**323,753**	**N**

3.2.2 Dynamic Case

As discussed in section 3.1.5, vortex shedding causes a response in the transverse direction, which is referred to as the cross-wind response. Response due to vortex shedding is difficult to quantify, and it depends on many factors including building geometry, wind speed, turbulence, and upwind effects on the building. However, from Equation 3.2, one can relate wind speed to the shedding frequency as follows,

$$V = \frac{fD}{S_T} \tag{3.5}$$

If the Strouhal number is assumed to be 0.2, and the shedding frequency is set to the building's natural frequency, the critical wind speed can be obtained. As an introductory analysis, the building's natural period can be approximated as N/10, where N is the number of stories. For a

40-story building, the natural period given by the rule of thumb is 4 seconds; hence a frequency of 0.25 Hz. Evaluating Equation 3.3 for a building width of 30 m gives a critical wind speed of 37.5 m/s. This wind speed is below the design wind speed of 47 m/s, signifying the building's vulnerability to dynamic resonant response at its fundamental mode due to vortex shedding.

Determining the exact pressure exerted on the sides of the building due to the formation of the vortices is difficult without wind tunnel testing. However, shedding pressure can be estimated as approximately half of the windward pressure. It is also reasonable to assume that this pressure will be applied to half of the nodal tributary area of the building. Another aspect of vortex shedding phenomenon to consider is the fact that vortices will not form uniformly at the same time throughout the height of the building. In reality the wind velocity profile is varying while the building geometry stays constant. Hence, it is safe to consider for analysis purpose that uniform shedding occurs throughout half the height of the building. With all these assumptions, the wind pressure due to vortex shedding can be taken as ¼ of the windward pressure applied to the full tributary area of the building. Therefore, the equivalent nodal point force for the discrete model is 23.8 kN.

CHAPTER 4: STATIC ANALYSIS OF SINGLE OUTRIGGER

4.1 Numerical Derivation

In general, a 3D analysis is necessary to examine the complete interaction among the different elements in the outrigger system. However, from the view of expense and time, a more general and robust optimization tool may be preferred in the early stages of the design phase. As such, a method based on simplifying assumptions is presented in this chapter to determine the optimal location of a single outrigger.

4.1.1 Assumptions

The core of the building is modeled as a cantilever beam with constant cross section and uniform stiffness throughout the height of the building. An infinitely rigid outrigger arm is attached to the core, therefore assuming that the core rotates the same amount as the outrigger. The perimeter columns are pinned to the ground with some initial tension. It is assumed that the applied loading is a quasi-static uniformly distributed wind load. An illustration of the simplified model is shown in Figure 8.

The two main constraints in the design of an outrigger system are the horizontal deflection at the top of the structure, and also the maximum moment generated at the base of the building. The maximum horizontal deflection needs to be below a tolerable limit of human comfort usually defined by $\alpha.H$, where α is in the order of 1/400 to 1/500, and H is the total height of the building. The base moment has no influence on occupant comfort, but has a great impact in the overall building cost as far as foundation system and member sizes are concerned.

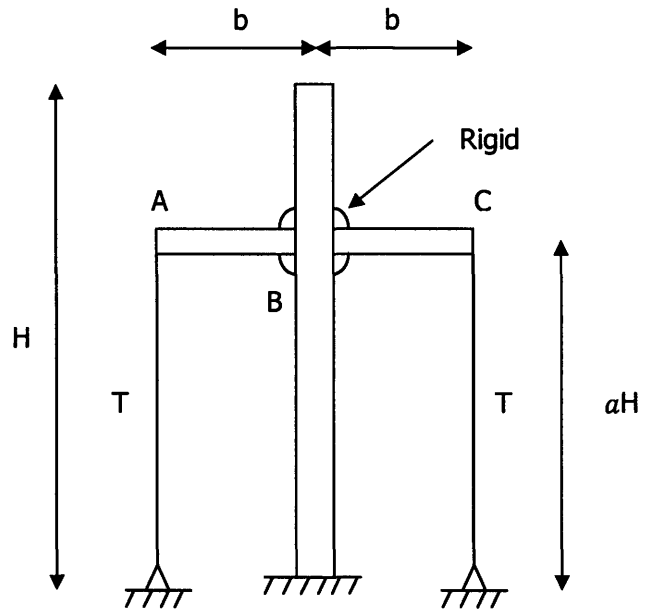

Figure 8: Simplified single outrigger model

4.1.2 The Basic Problem

First, consider a simple cantilever beam subjected to uniform loading (see Figure 9).

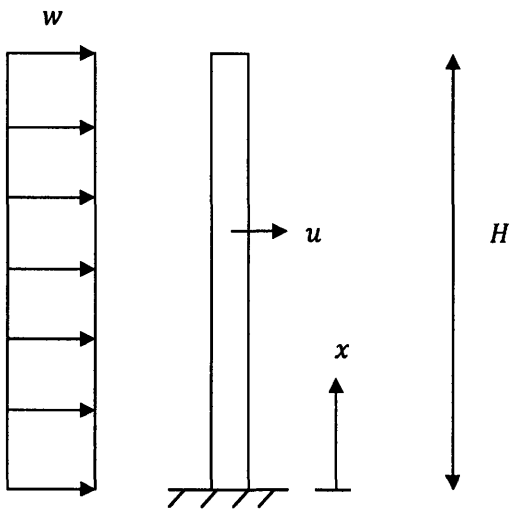

Figure 9: Cantilever subjected to uniform loading

The deflection profile is given by

$$u(x) = \frac{wx^2}{24EI}(6H^2 - 4Hx + x^2) \tag{4.1}$$

Hence, the deflection at the top is

$$u(H) = \frac{wH^4}{8EI} \tag{4.2}$$

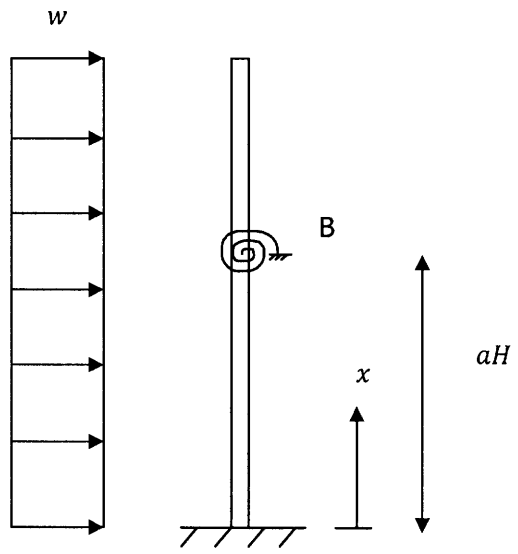

Figure 10: Cantilever beam with rotational spring

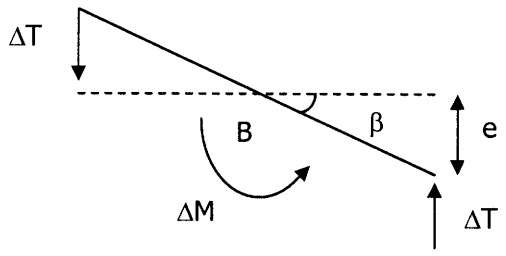

Figure 11: Free body diagram of the displaced outrigger arm

Now, the outrigger is modeled as a rotational spring located at point B (see Figure 10). To obtain the rotational stiffness, K_R , a rotation β is applied at point B (see Figure 11). The extension in the column, $e = b\beta$, and the change in moment can be written as

$$\Delta M = 2b\Delta T \tag{4.3}$$

where,

$$\Delta T = \frac{AE_{col}}{aH} e = \frac{AE_{col}}{aH} b\beta \tag{4.4}$$

Thus,

$$\Delta M = \left(\frac{2b^2 AE_{col}}{aH}\right)\beta = K_R\beta \tag{4.5}$$

$$K_R = \left(\frac{2b^2 AE_{col}}{aH}\right) \tag{4.6}$$

Knowing the rotational stiffness, K_R , one can find the moment in the spring, M_S , by satisfying the rotational compatibility condition at location aH. The final rotation of the cantilever is

$$\beta_f = \beta_c - \beta_s \tag{4.7}$$

where, β_c = rotation of the cantilever at $x = aH$ due to uniform lateral load w

β_s = rotation due to the rotational spring restraint located at $x = aH$

(The negative sign indicates that the rotation of the cantilever due to the spring stiffness acts in a direction opposite to the rotation due to external load)

The slope equation of a cantilever beam subjected to uniform loading is the derivative of its deflection profile, and is given by

$$\beta(x) = \frac{wx}{6EI}(3H^2 - 3Hx + x^2) \tag{4.8}$$

$$\beta_c = \beta(aH) = \frac{waH^3}{2EI}\left(1 - a - \frac{a^2}{3}\right) \tag{4.9}$$

$$\beta_s = \int_0^{a.H} \frac{M_s}{EI} dx = \frac{M_s aH}{EI} \tag{4.10}$$

and

$$\beta_f = \frac{M_s}{K_R} \tag{4.11}$$

Hence, Equation 4.7 yields the following

$$\frac{M_s}{K_R} = \beta(aH) - \frac{M_s aH}{EI} \tag{4.12}$$

Substituting known variables and simplifying the expression, one obtains

$$M_S = \frac{wH^2}{2}\left[\frac{1 - a - \frac{a^2}{3}}{1 + \frac{EI}{2b^2 AE_{col}}}\right] = f\left(\frac{wH^2}{2}\right) \tag{4.13}$$

where,

$$f = \frac{1 - a - \frac{a^2}{3}}{1 + \frac{EI}{2b^2 AE_{col}}} \tag{4.14}$$

The resulting moment diagram is shown in Figure 12.

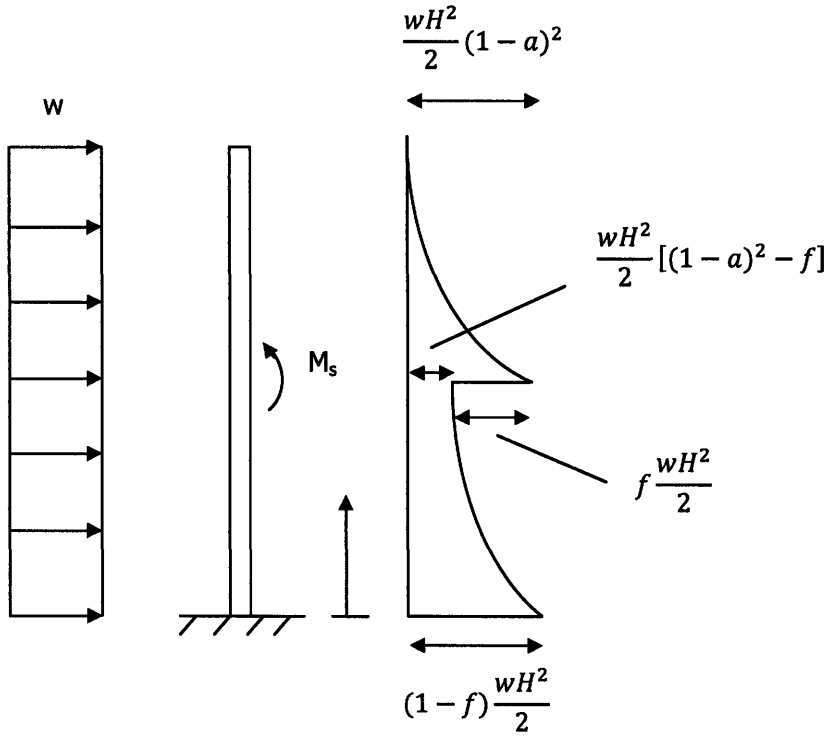

Figure 12: Moment diagram due to outrigger

4.1.3 Optimal Outrigger Location

The optimal location of a single outrigger is one that achieves a balanced moment design. This means that the reduction of moment is such that the base moment is equal to the moment at the level just above the outrigger, in other words, right before the counter moment takes effect. From the design perspective, this is desirable because the properties of the core can be designed uniformly throughout the height of the building to provide adequate amount of stiffness at both levels. If the moments at the two levels are imbalanced, one of the two moments will dominate the other, and the resulting design moment will be greater than what is obtained from a balanced design.

To generate an analytical solution for the optimum location, the two expressions of the base moment and the moment at the outrigger level are set equal to each other.

$$(1-f)\frac{wH^2}{2} \equiv \frac{wH^2}{2}(1-a)^2$$

$$1-f \equiv 1-2a+a^2$$

$$f \equiv a(2-a) \tag{4.15}$$

Note that the condition $(1-a)^2 - f \geq 0$ needs to be satisfied so that the moment reduction does not exceed the available moment.

Therefore,

$$\frac{1-a-\frac{a^2}{3}}{1+\frac{EI}{2b^2AE_{col}}} \equiv a(2-a) \tag{4.16}$$

Finally, solving the quadratic equation in a yields the following

$$a = \frac{9b^2AE_{col} + 3IE - \sqrt{57b^4A^2{E_{col}}^2 + 36Ib^2AE_{col}E - 9E^2}}{4b^2AE_{col} + 3IE} \tag{4.17}$$

where a = parameter that represents a fraction of the total height of the core

b = length of the outrigger arm

A = area of the perimeter column, and

I = moment of inertia of the core

4.1.4 Horizontal Deflection at Top

The deflection at the top of a cantilever beam is given by Equation 4.2. Thus, the horizontal deflection at the building top with the outrigger system attached is simply the superposition of the deflection of the cantilever beam due to the uniform load and the deflection due to the moment induced by the rotational spring.

$$u(H) = \frac{wH^4}{8EI} - \left[\int_0^{aH} \frac{M_S x}{EI} dx + \int_{aH}^{H} \frac{M_S aH}{EI} dx\right] \tag{4.18}$$

$$u(H) = \frac{wH^4}{8EI} - \frac{M_S}{2EI}(aH)^2 - \frac{M_S aH}{EI}(H - aH)$$

$$u(H) = \frac{wH^4}{8EI}\{1 - f[4a(1-a) + 2a^2]\} \tag{4.19}$$

For design purpose, $u(H) < \alpha H$ should be satisfied.

Therefore,

$$\frac{wH^3}{8EI}\{1 - f[4a(1-a) + 2a^2]\} < \alpha \tag{4.20}$$

In balanced moment design, substituting Equation 4.15 into Equation 4.20 gives

$$\frac{wH^3}{8EI}\{1 - 2a^2(2-a)^2\} < \alpha \tag{4.21}$$

4.2 Applying Outrigger Effect to Discrete Model

Procedure to generate the mass and stiffness matrix for the building core has been described in Chapter 2. The next step is to introduce the effect of the outrigger. For the case of no damping, the differential equation of motion reduces to

$$\boldsymbol{M\ddot{U} + KU = P} \tag{4.22}$$

The effect of the outrigger can be modeled by introducing a minor change in the stiffness matrix. Similar to what is done in the analytical case, a rotational spring is to be added to the nodal point where the outrigger is located. Hence, the outrigger nodal point will have a modified rotational stiffness comprised of the existing rotational stiffness from the core (cantilever beam) and the rotational stiffness K_R from the outrigger. The value of K_R is the obtained in the same way outlined in section 4.1.2.

In the case of a damped outrigger, the damping matrix, C, is required to solve the full differential equation of motion

$$\boldsymbol{M\ddot{U} + C\dot{U} + KU = P} \tag{4.23}$$

The conventional approach is to work in the real domain by constructing the damping matrix and introducing the damping coefficient c at the location corresponding to the rotation of the outrigger node. However, it is algebraically more convenient to work in the complex domain, by collapsing the C matrix altogether and lumping the effect of damping into the stiffness matrix, forming an equivalent complex stiffness matrix. This will be discussed further in detail in Chapter 5.

4.3 Analytical Solution vs. Discrete Model

Before proceeding any further with analysis, it is important to ensure that the discrete model matches the analytical solution with reasonable accuracy. The first step is to check the pure cantilever beam solution for horizontal top deflection. Using a uniformly distributed load of 40 nodal point forces divided the total height, the analytical solution gives a value of 0.3981 m. The discrete model solution with point forces applied at nodal points gives a value of 0.4115 m. This corresponds to a percent error of 3.3% which is considered tolerable for an analysis of this scale. Furthermore, the discrete solution gives a higher deflection value which contributes to a more conservative design.

Applying Equation 4.17 to the proposed 40-story building gives an optimal outrigger location of 52.65% of the height from the ground. This corresponds most closely to story number 21. The discrete model can then be modified to accommodate for an outrigger at the 21^{st} story for a fair comparison. The analytical solution for this case from Equation 4.19 gives a value of 0.3326 m while the discrete solution gives a value of 0.3438 m. Again the percent error is 3.3% which shows consistency in the model.

CHAPTER 5: THE DAMPED OUTRIGGER CONCEPT

The preceding chapters have described how an outrigger system works. This chapter will present a variant of the system in which viscous damper elements are introduced into the load paths in order to create dynamic stiffness in the form of damping resistance. By introducing these damping elements, some static stiffness and strength may be forfeited. However, if the damping generated is significant, the reduction in dynamic lateral response will more than compensate for the reduction in static stiffness and strength, resulting is a more economical design.

5.1 Overview of the Damped Outrigger System

Figure 13 shows how the system works on a core-to-perimeter column outrigger system. A relative vertical motion between the perimeter columns and the ends of the stiff outriggers cantilevering from the core is generated as the building undergoes dynamic sway motion. Viscous dampers are inserted across this structural discontinuity to dissipate energy during the cyclic motion, resulting in the increase of the overall damping of the building.

A typical detail of the dampers at the outrigger level is shown in Figure 14. Although only two damping components are shown in the diagram, it is possibly more economical to supply damping resistance in the form of a number of smaller components to increase the redundancy of the system. The outrigger link has to be rigid enough to ensure that it moves vertically relative to the floors at these levels. The floors will naturally bend in double curvature to remain connected to the core and the outer columns. The entire arrangement at the outrigger level can be seen in Figure 15.

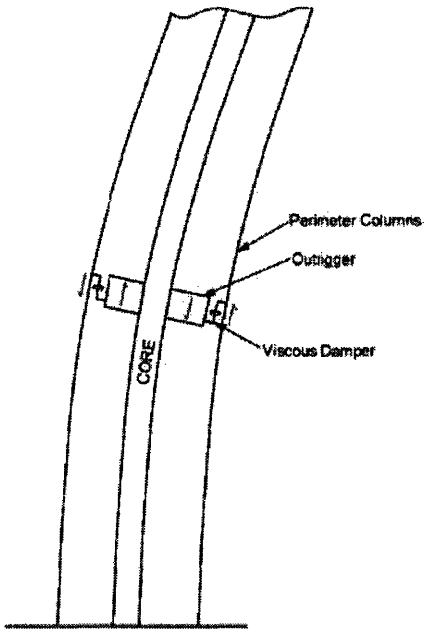

Figure 13: Damped outrigger concept (Smith & Willford, 2007)

The actual performance of the damped outrigger system is dependent on a number of factors listed below (Smith & Willford, 2007):

- The flexural and shear rigidities of the core and wall elements
- The axial stiffness of the perimeter columns and the distance from the core
- The number of outriggers and their stiffness
- The stiffness of the floor beams spanning between the core to the perimeter
- The stiffness of other elements of the lateral resisting system, e.g. perimeter frame action

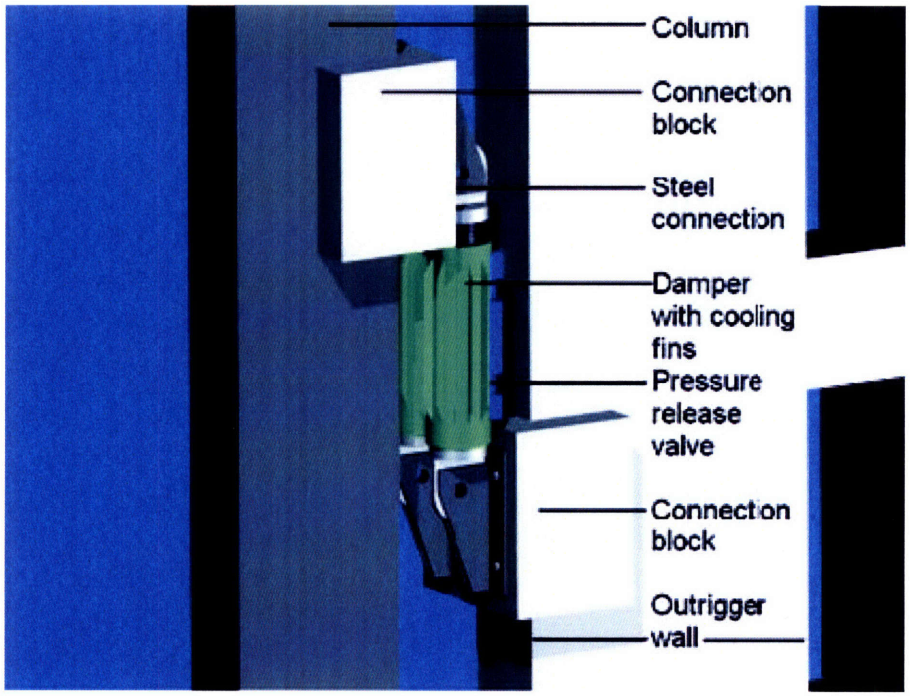

Figure 14: Conceptual detail at outrigger level (Smith & Willford, 2007)

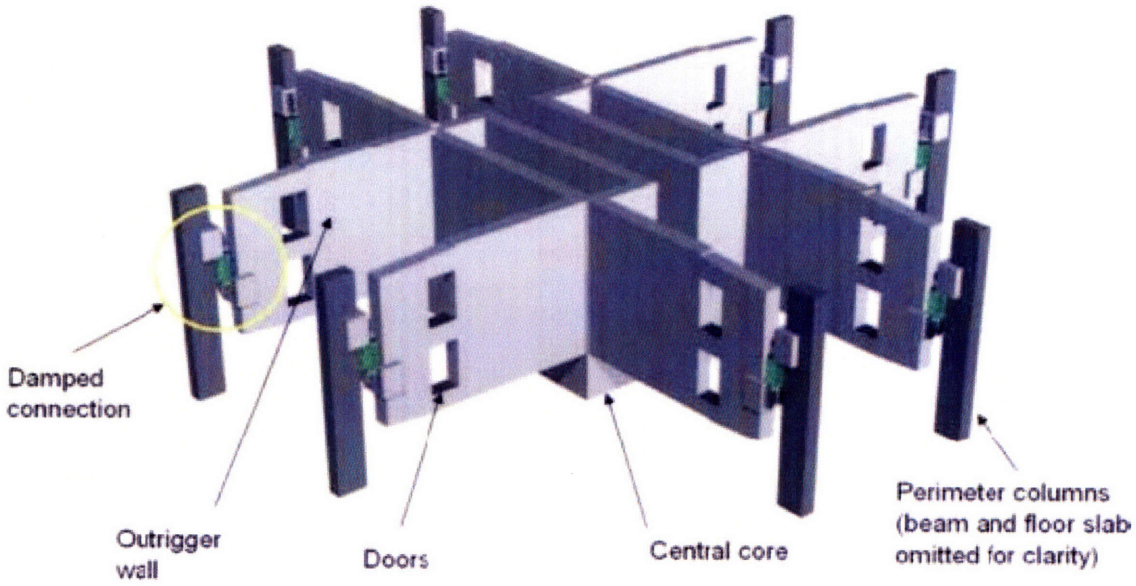

Figure 15: Typical layout at outrigger levels (Smith & Willford, 2007)

5.2 Derivation of Equivalent Complex Stiffness

The damped outrigger system can be modeled in a similar way as a regular outrigger system. However, a dashpot representing the fluid viscous damper is added at the connection between the end of the outrigger and the perimeter column. While the concept presented by Smith and Willford implies that the damper is in series with the perimeter column, parallel configuration of damper and column will also be studied in this thesis to provide a good comparative study. The simplified model of the damped outrigger concepts are illustrated in Figure 16.

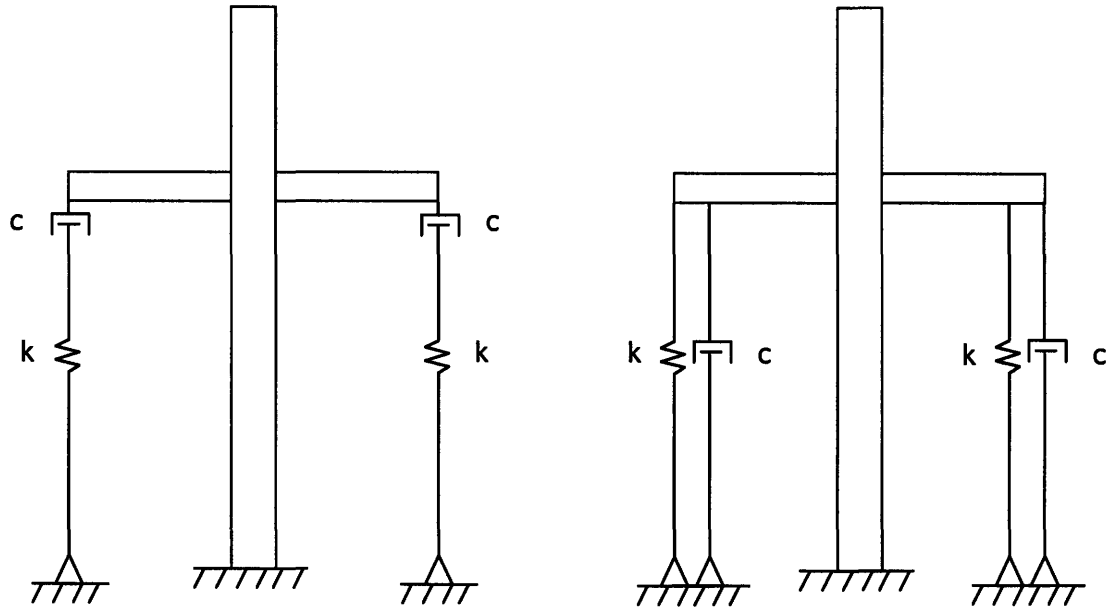

Figure 16: Simplified model of damped outriggers in series (left) and in parallel (right)

As mentioned in Chapter 4, damping introduces complexity to the solution by adding a term involving velocity. In order to obtain the equivalent complex stiffness, a harmonic excitation is applied to a 1-dof system for both parallel and series configuration, and the governing equations is written in terms of complex quantities.

5.2.1 Damper in Parallel

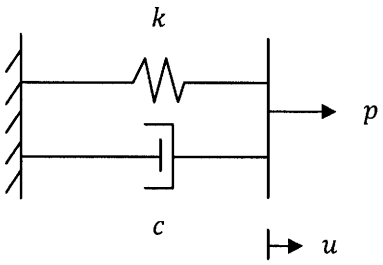

Figure 17: Damper in parallel

$$p = \hat{p}e^{iwt}$$

$$u = \tilde{u}e^{iwt}$$

$$\hat{p} = ku + c\dot{u}$$

$$\hat{p} = (k + iwc)\tilde{u} = k_{eq}\tilde{u}$$

$$k_{eq} = (k + iwc) = \hat{k}e^{i\varphi} \tag{5.1}$$

$$\tilde{u} = \frac{\hat{p}}{k_{eq}} = \frac{\hat{p}}{\hat{k}}e^{-i\varphi}$$

$$u = \tilde{u}e^{iwt} = \tilde{u}e^{i(wt-\varphi)}$$

5.2.2 Damper in Series

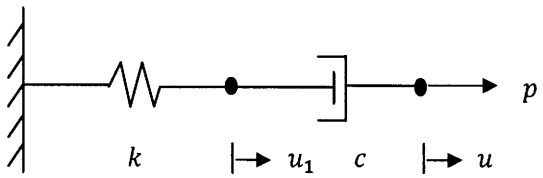

Figure 18: Damper in series

$$p = \hat{p}e^{iwt}$$

$$u = \tilde{u}e^{iwt}$$

$$u_1 = \tilde{u}_1 e^{iwt}$$

$$\hat{p} = ku_1 = c(\dot{u} - \dot{u_1})$$

$$(iwc)\tilde{u} = (k + iwc)\tilde{u}_1$$

$$\tilde{u}_1 = \frac{iwc}{k + iwc}\tilde{u}$$

$$\hat{p} = \frac{kiwc}{k + iwc}\tilde{u} = k_{eq}\tilde{u}$$

$$k_{eq} = \frac{kiwc}{k + iwc} = \hat{k}e^{i\varphi} \qquad (5.2)$$

$$\tilde{u} = \frac{\hat{p}}{k_{eq}} = \frac{\hat{p}}{\hat{k}}e^{-i\varphi}$$

$$u = \tilde{u}e^{iwt} = \tilde{u}e^{i(wt-\varphi)}$$

The equivalent complex stiffness has been derived for both series and parallel damper configurations. The next step is to incorporate this effect into the stiffness matrix of the core. The force exerted by the perimeter column on the outrigger link is

$$\hat{p} = k_{eq}\tilde{u} \tag{5.3}$$

Hence, as previously done in Chapter 4, the addition of rotational stiffness to the core at the outrigger level can be obtained as follows (see Figure 19)

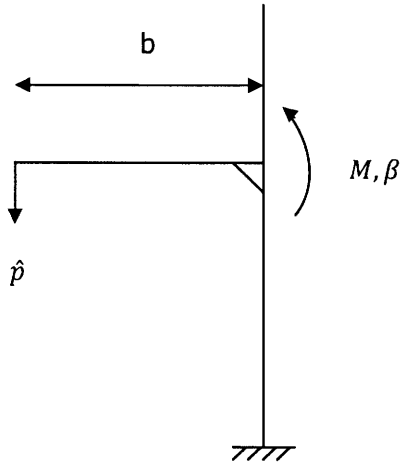

Figure 19: Outrigger force diagram

$$M = b\hat{p}$$

$$M = bk_{eq}\tilde{u}$$

$$\tilde{u} = \mathrm{b}\beta$$

$$M = k_{eq}\mathrm{b}^2\beta = K_R\beta$$

$$\therefore K_R = k_{eq}\mathrm{b}^2 \tag{5.4}$$

5.3 Static Analysis

The variant outrigger systems employ the use of viscous dampers; however, dampers require motion (velocity) in order for it to function. Under steady state wind, whereby the load is applied slowly onto the structure, the variant outrigger systems should behave as if no dampers are present. In order to confirm this, the discrete model is run in MATLAB for 4 different configurations: (1) outrigger with damper in series, (2) outrigger with damper in parallel, (3) outrigger without damper, and (4) a base system without any outrigger. For discussion purpose, the different configurations will be referred to by their numbers. For configurations (1) and (2), the forcing frequency ω is set to zero to represent a static case. The matrix equation to be solved is

$$\boldsymbol{K_{eq}U = P} \tag{5.5}$$

Figure 20 shows the horizontal displacement profile of the building along the height. It can be seen that the points for configuration (1) coincide with the curve of configuration (4), and the points for configuration (2) coincide with the curve of configuration (3). Configurations (1) and (4) produce a horizontal displacement at the 40^{th} story of 0.41 m. This suggests that the outrigger system with series damping behaves exactly the same as a system without outriggers under static loading. When there is no force in the damper due to the lack of motion, the perimeter column attached under it will also experience no force based on force compatibility. Thus, no additional stiffness is provided by the outrigger under this configuration. On the other hand, configurations (2) and (3) experience a horizontal top deflection of 0.34 m. This implies that the outrigger with parallel damping configuration behaves as a regular outrigger under static load. Mathematically, it can be shown that as $\omega \to 0$

$$k_{eq}\ (series) = \frac{kiwc}{k + iwc} \to 0$$

$$k_{eq}\ (parallel) = k + iwc \to k$$

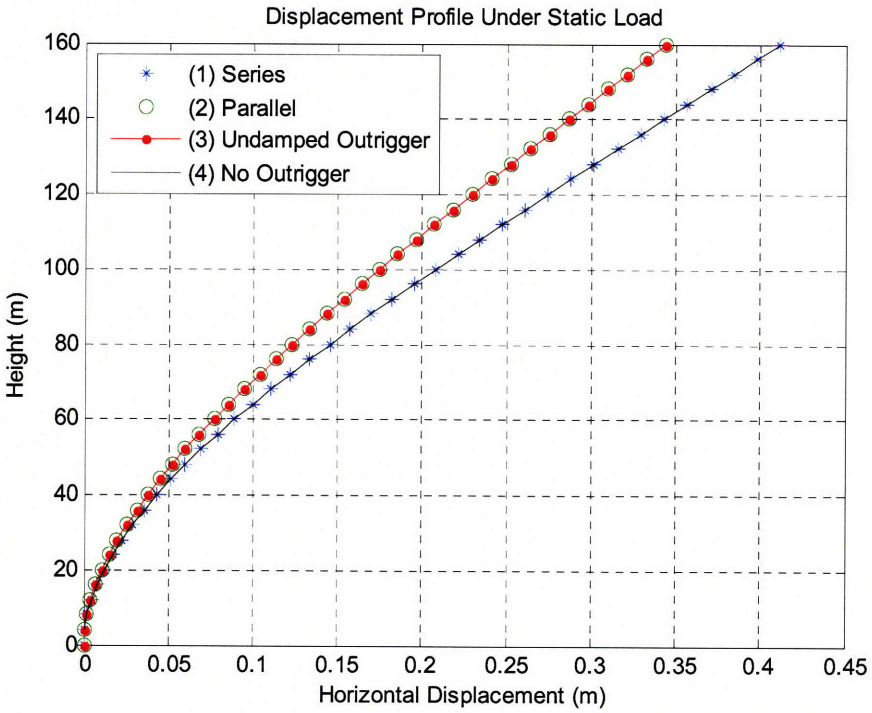

Figure 20: Plot of displacement profile under static loading

For a building 160 m tall, the maximum horizontal deflection permitted by the code is in the order of $H/400$, where H is the total height of the building. Under this rule, the top floor is allowed a maximum deflection of 0.4 m. For this particular building, only configurations (2) and (3) will be able to pass the requirement, while configurations (1) and (4) are slightly off the limit. The outrigger system proves to be useful in this situation, allowing a reduction in deflection of approximately 17%. Without the use of outriggers, the core walls have to be thickened all the way through the height of the building which is often undesirable in terms of materials and space.

5.4 Dynamic Analysis

5.4.1 Modal Analysis

In order to analyze the dynamic response of the building due to cross-wind excitation, it is customary to first determine the natural period of vibration of the building as well as its mode shapes. This is achieved by solving the eigenvalue problem of the form

$$\boldsymbol{K\varphi} = \omega^2 \boldsymbol{M\varphi} \tag{5.6}$$

where $\boldsymbol{\varphi}$, the eigenvectors, represent the mode shape and the eigenvalues correspond to ω^2. The natural period of the building can then be obtained from the relationship

$$T = \frac{2\pi}{\omega} \tag{5.7}$$

In the previous section, under static loading, it is observed that the outrigger with damper in series behaves essentially the same as a system without outrigger. On the other hand, the outrigger with damper in parallel behaves the same as a regular outrigger. Similarly, the natural period of the system follows the same relationship since it is independent of damping. Table 2 summarizes the frequencies and periods of the first three modes for the two variant outrigger systems. The fundamental period is found to be 3.91 seconds for the series configuration and 3.58 seconds for the parallel configuration of dampers. This is fairly close to 4 seconds given by the approximate rule of thumb of N/10, where N is the number of stories. The frequencies for the fundamental mode show a difference of approximately 9% between the two configurations. This illustrates the fact that the outrigger has caused an increase in stiffness in the system, therefore raising the fundamental frequency of the building.

Table 2: Frequency and period of first three modes

	Mode	Series	Parallel
Frequency, ω (rad/sec)	1	1.606	1.757
	2	9.994	10.003
	3	27.655	27.846
Period, T (seconds)	1	3.912	3.576
	2	0.629	0.628
	3	0.227	0.226

With regards to the higher modes (second and third), the frequencies in both systems are fairly close to each other. Also, it is unlikely that these modes will be excited under normal loading conditions for civil structures. The fundamental mode, however, has a period that is very prone to resonant loading from gust effect and vortex shedding. Figure 21 displays the mode shapes for the first three modes of vibration. The number of zero inflection points in the mode of vibration is n-1, where n is the mode number.

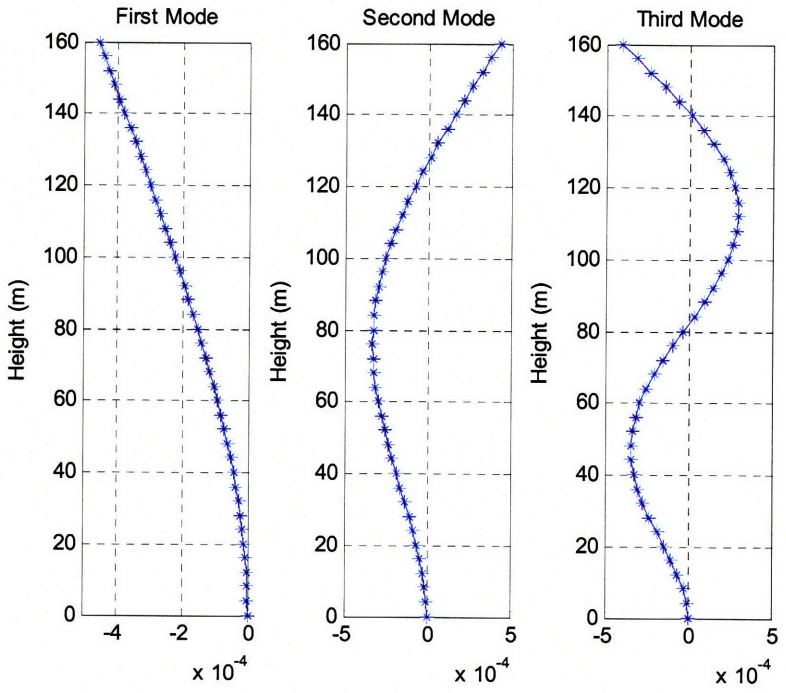

Figure 21: Mode shapes of first three modes

5.4.2 Response Function

The modal properties of the building have been determined in the previous section. To obtain the response function of the structure due to cross-wind dynamic excitation, a frequency-based approach will be used. A complex periodic loading function will be applied to the building in the form of $p = \hat{p}e^{iwt}$. In this approach, the quantity of interest is the variation of the amplitude of vibration with frequency. In order to determine the amplitude of vibration, the equation of motion is written as follows

$$m\ddot{u} + k_{eq}u = \hat{p}e^{iwt} \tag{5.8}$$

Equation 5.8 allows a particular solution of the form

$$u = \tilde{u}e^{iwt} \tag{5.9}$$

The time derivatives of Equation 5.9 are

$$\dot{u} = i\omega\tilde{u}e^{iwt} \tag{5.10}$$

$$\ddot{u} = -\omega^2\tilde{u}e^{iwt} \tag{5.11}$$

Substituting Equations 5.10 and 5.11 into the differential equation, factoring the common term $\tilde{u}$ and cancelling the common (non-zero) exponential term on either side yields

$$(k_{eq} - \omega^2 m)\tilde{u} = \hat{p} \tag{5.12}$$

To simplify the expression, the quantity $\hat{k}$ is defined as follows

$$\hat{k} = (k_{eq} - \omega^2 m) \tag{5.13}$$

Hence, in matrix form, Equation 5.12 becomes

$$\hat{k}\tilde{u} = \hat{p} \tag{5.14}$$

Finally, the displacement matrix is given by

$$\tilde{u} = \hat{k}^{-1}\hat{p} \tag{5.15}$$

For analysis purpose, the governing deflection parameter is the maximum drift at the top of the structure, in this case, the deflection at the 40th floor/node. Recall from section 5.2 that k_{eq} is a complex quantity due to contribution from damping. Therefore, the displacement parameter $\tilde{u}_{40}$ also contains real and imaginary parts. The amplitude of vibration is obtained by taking the sum of the squares of the real and imaginary part, then taking the square root.

$$|\tilde{u}_{40}| = \sqrt{(\tilde{u}_{40})_{real}{}^2 + (\tilde{u}_{40})_{imaginary}{}^2} \tag{5.16}$$

The frequency-based response function for the building, ω vs. $|\tilde{u}_{40}|$, is shown in Figure 22. Alternatively, the response function plotted with respect to period can be seen in Figure 23. The range of ω is set to be from 0-30 rad/sec to cover the first three modes. These plots are obtained using a loading magnitude of 23.8 kN at each node (as derived in Chapter 3) and a damping coefficient of 100,000 kN.s/m. Three resonant responses can be observed from both plots, corresponding to the frequency or period of the three fundamental modes of vibration. The second and third mode resonant response occur over a very narrow band of frequency, hence it is very difficult to excite these modes continuously. Furthermore, as previously mentioned, wind excitation does not generally have as frequency of 10 rad/sec or more. From here onwards, the focus of the analysis will be on the fundamental mode resonant response.

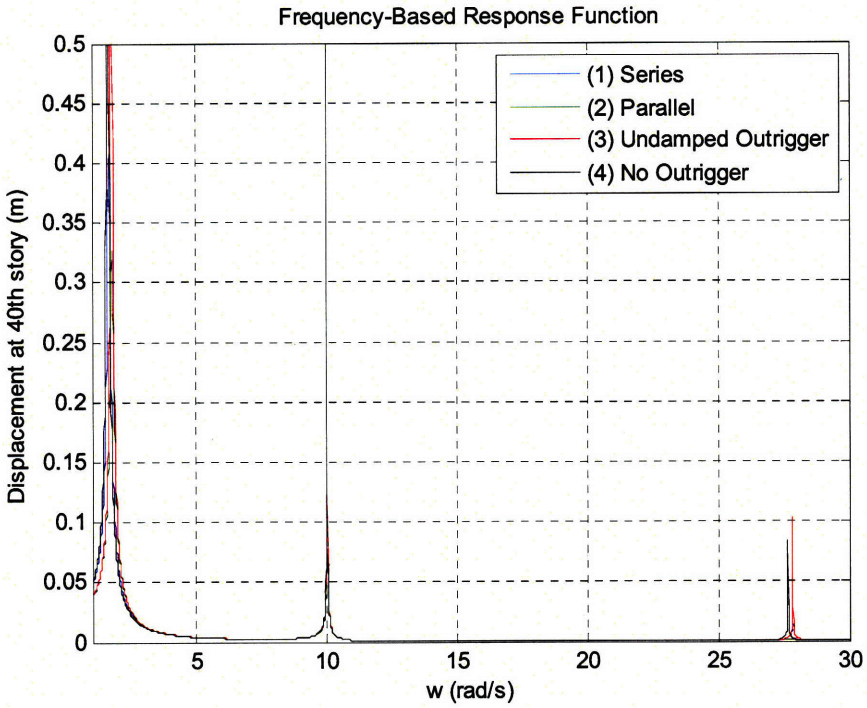

Figure 22: Frequency-based response function

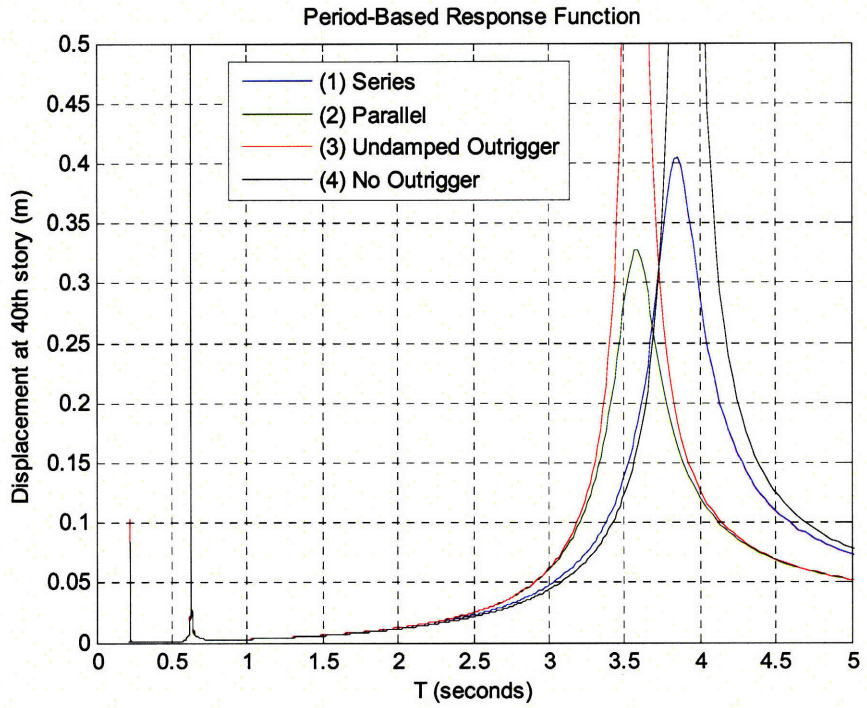

Figure 23: Period-based response function

Figure 24 shows a zoomed version of Figure 22, limiting the frequency range to between 1.1 – 2.2 rad/sec. Configurations (3) and (4) blow up to infinity at the fundamental frequency of the corresponding systems, as expected for undamped systems. It is also observed that the peak response for configuration (1) occurs around the fundamental frequency of configuration (4), and the peak response of configuration (2) occurs around the fundamental frequency of configuration (3), again consistent with previous findings. Under the reduced load of 23.8 kN and damping coefficient of 100,000 kN.s/m, the peak response for configuration (1) exceeds 0.4 m, which is the maximum permissible displacement by the code. On the other hand, configuration (2) produces a peak displacement below the maximum threshold. From first observation, configuration (2) seems to perform better than configuration (1) in terms of the maximum displacement experienced by the structure.

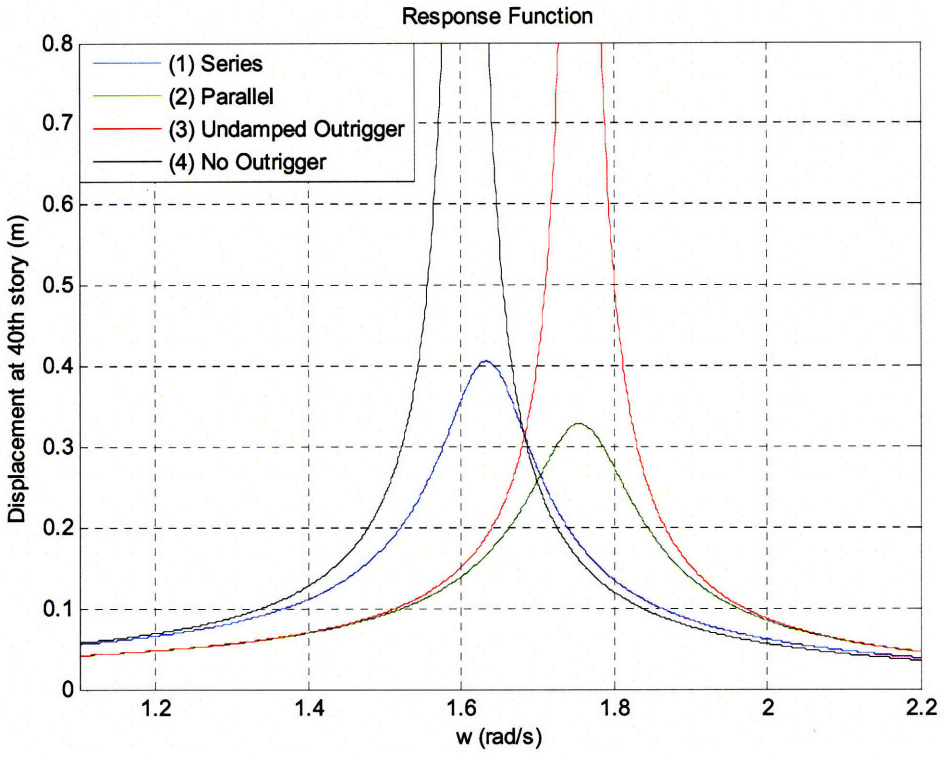

Figure 24: Frequency-based response function zoomed at fundamental mode

5.4.3 Acceleration & Motion Perception

Wind induced oscillation in structures can lead to structural failure when the amplitude is large. Although buildings are commonly designed to prevent structural damage, small oscillations in the building that are not large enough to cause structural damage, may induce human discomfort. Especially in tall buildings, it is important to design the structure such that it will not only resist structural damage, but also to keep the building motion under comfortable limits of occupants. Keeping building motion within acceptable limits is often found as more of a challenge than ensuring that the building has sufficient stiffness.

The horizontal force experienced by an occupant in a building is a function of the horizontal acceleration; hence acceleration has become a common index of measuring motion effects. For civil structures, acceleration is more commonly measured in terms of milli-g (one thousandth of gravity). From experimental results, people can be sensitive to accelerations as small as a few milli-g. Designing a building for zero motion will be unrealistic and too expensive, therefore, a guideline defining the maximum permissible acceleration is required.

The International Standards Organization (ISO) has published guidelines of acceleration values at the top of the building that should not be exceeded for a return period of 5 years. The criteria are primarily applicable to office buildings since most data are available for that particular case. Figure 25 illustrates the acceleration criteria taken from ISO, plotted against the natural period of the building. The building analyzed in this thesis has a natural period of about 4 seconds, therefore, reading directly from the graph, the maximum allowed acceleration at the top of the building is roughly 15 milli-g (0.147 m/s^2).

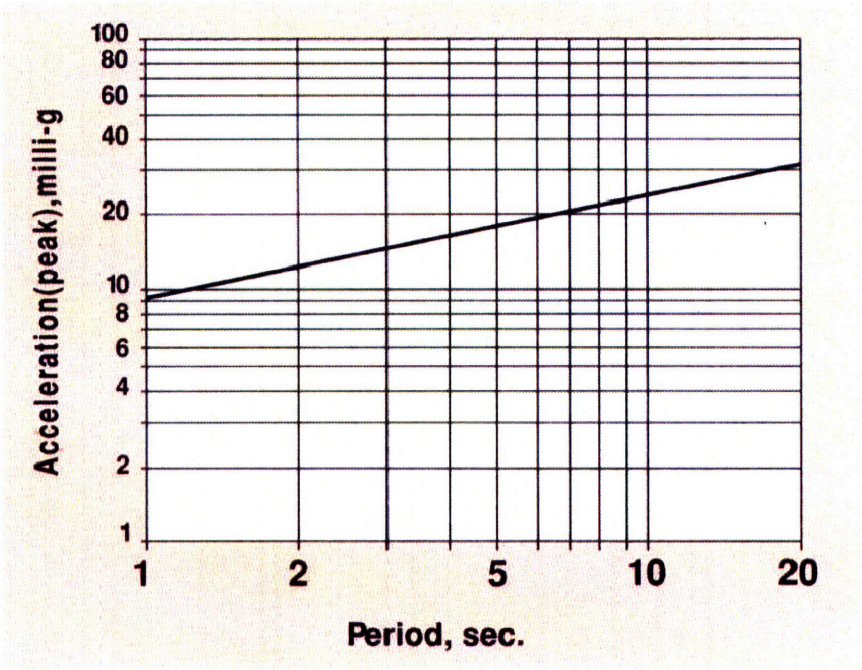

Figure 25: Guideline for 5 year acceleration in buildings (RWDI Inc., 2008)

To obtain the acceleration at the 40th story under fundamental mode resonant response, recall that the solution of the differential equation of motion has the form:

$$u = \tilde{u}e^{i(\omega t-\delta)} \tag{5.17}$$

The acceleration function is the second derivative of the displacement function, which is

$$a = \ddot{u} = -\omega^2\tilde{u}e^{i(\omega t-\delta)} \tag{5.18}$$

This means that the magnitude of acceleration at the 40th story is simply

$$|a_{40}| = \omega^2|\tilde{u}_{40}| \tag{5.19}$$

If ω is taken as the frequency at resonance, it follows that the maximum acceleration for configurations (1) and (2) are 1.05 m/sec^2 and 1.01 m/sec^2 (~0.1g) respectively. As such, both configurations (1) and (2) exceed the motion criteria at resonance.

5.4.4 The Half-Power Bandwidth Method

The percent of critical damping provided by the two configurations of dampers can be obtained by using the half-power bandwidth method. Other method such as the logarithmic decrement method only applies to single degree of freedom systems. The half-power bandwidth method is a procedure to determine experimentally the damping ratio in lightly damped structures. The procedure is to excite the dynamic system near resonance and then monitoring the amplitude of harmonic response. The maximum peak displacement is recorded and the frequencies ω_1 and ω_2 at which the response is $\sqrt{2}/2$ (70.7%) of the peak is measured. The fraction of critical damping is then given by the following formula

$$\xi = \frac{\omega_2 - \omega_1}{\omega_2 + \omega_1} \tag{5.20}$$

Pictorially, the procedure is illustrated in the diagram in Figure 26.

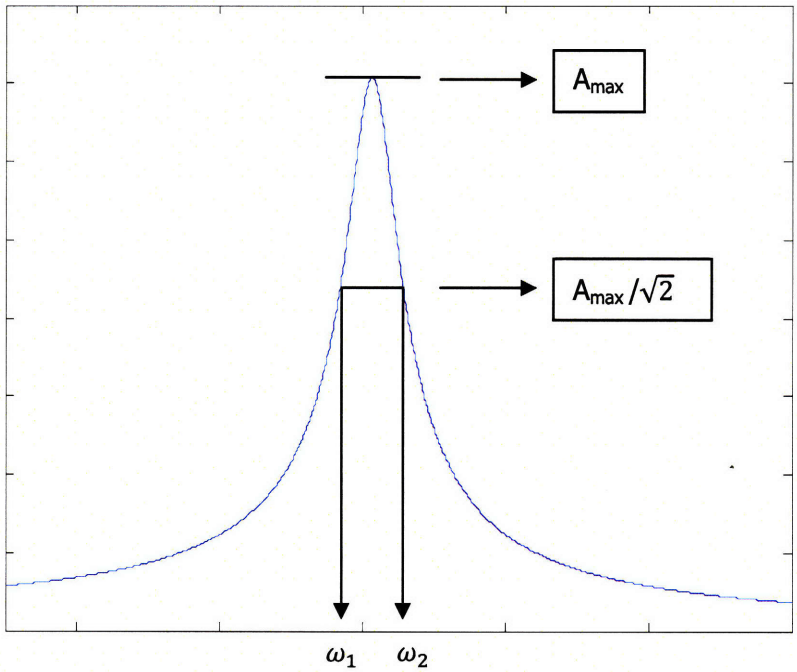

Figure 26: Half power bandwidth method

5.4.5 Effect of c on % damping

In section 5.4.2, it is observed that the parallel placement of viscous damper result in lower amplitude of vibration compared to when the damper is in series. Although the same damping coefficient value is used in both configurations, the two systems may not give the same overall building damping. To investigate the relationship between the amount of damping installed with respect to the overall % damping of the system, response functions were generated with different values of damping coefficient, c, and the corresponding fraction of critical damping, ξ, is obtained by implementing the half-power bandwidth method in MATLAB. The result is shown in Table 3.

Table 3: Equivalent building damping for various damper setting

	ξ		% damping	
c (kN.s/m)	**Series**	**Parallel**	**Series**	**Parallel**
10,000	0.0044	0.0040	0.44	0.40
50,000	0.0217	0.0196	2.17	1.96
80,000	0.0320	0.0316	3.20	3.16
90,000	0.0350	0.0353	3.50	3.53
100,000	0.0377	0.0393	3.77	3.93
150,000	0.0456	0.0594	4.56	5.94
200,000	0.0471	0.0799	4.71	7.99
250,000	0.0451	0.1004	4.51	10.04
300,000	0.0418	0.1220	4.18	12.20
350,000	0.0383	0.1445	3.83	14.45
400,000	0.035	0.1681	3.50	16.81
450,000	0.032	0.1929	3.20	19.29
500,000	0.0293	0.2193	2.93	21.93

As expected, for c = 100,000 kN.s/m, the configuration in parallel provides a higher damping ratio compared to the series configuration. The relationship of c vs. % damping is almost linear for parallel configuration, whereas a more interesting behavior is observed for the configuration

in series. Initially, for c less than 90,000 kN.s/m, the series configuration provides a slightly better damping ratio than parallel configuration. However, the effectiveness of damping reaches its peak at around c = 200,000 kN.m/s, whereby a maximum percent damping of 4.71% is obtained. As further damping is introduced beyond this point, the configuration in series gradually loses its effectiveness as seen by the decrease in overall % building damping. Figure 27 illustrates this phenomenon whereby the maximum percent damping capable of being achieved by the series configuration is just under 5% critical. On the other hand, parallel configuration can continue to provide damping effectively as c is increased further than this point. Even so, 5% critical is a fairly high amount of damping compared to what is normally achieved using a tuned mass damper, considering only one outrigger level is utilized.

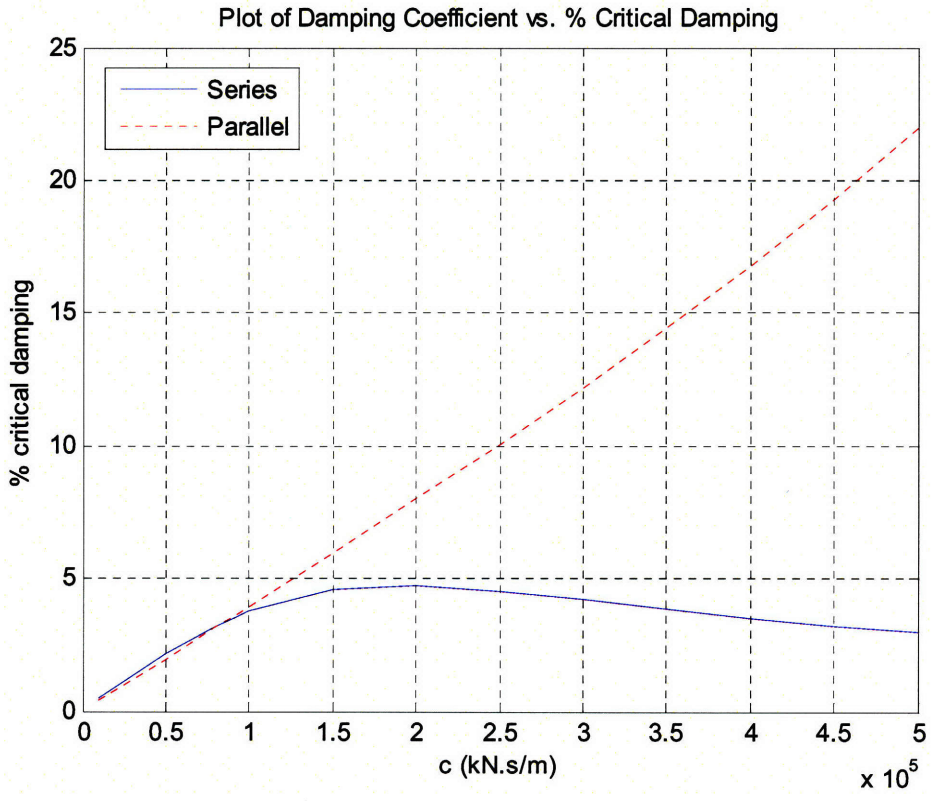

Figure 27: Plot showing relationship between c and critical damping

5.4.6 Analysis of 1-DOF System in Series

The objective of this section is to study the physical phenomenon of a damping system in series using a simpler and better understood 1 degree of freedom (dof) model. The curve given in Figure 27 in the previous section gives us an indication that a maximum critical damping point exist for the full scale 40-story discrete model. Although it is possible that the behavior is affected by several factors, one can postulate that the effect is entirely attributed to the damper placement; therefore studying a 1-dof model will help confirm this observation.

To derive the governing response equation for a spring, mass, damper system in series (see Figure 28), it is simplest to utilize the approach of equivalent stiffness from section 5.2. Extending the derivation presented in section 5.4.2 for a 1-dof system, one proceeds as follows

$$m\ddot{u} + k_{eq}u = \hat{p}e^{iwt} \tag{5.21}$$

Substituting a solution of the form $u = \tilde{u}e^{i\omega t}$ gives

$$(-\omega^2 m + k_{eq})\tilde{u} = \hat{p} \tag{5.22}$$

$$\tilde{u} = \hat{p}\left[\frac{1}{k_{eq} - \omega^2 m}\right] = \hat{p}\left[\frac{1}{\frac{ki\omega c}{k + i\omega c} - \omega^2 m}\right]$$

$$\tilde{u} = \hat{p}\left[\frac{1}{\frac{ki\omega c - \omega^2 m(k + i\omega c)}{k + i\omega c}}\right]$$

$$\tilde{u} = \hat{p}\left[\frac{k + i\omega c}{-\omega^2 mk + i(k\omega c - \omega^3 cm)}\right] \tag{5.23}$$

$$\tilde{u} = \hat{p}\, H(\omega)$$

The parameter, $H(\omega)$, which is the response function for a unit harmonic load ($\hat{p} = 1$) is known as the transfer function. At this point, consider the polar representation of a ratio of two complex numbers:

$$\frac{z_1}{z_2} = \frac{x_1 + iy_1}{x_1 + iy_2} = \frac{r_1 e^{i\delta_1}}{r_2 e^{i\delta_2}} = \frac{\sqrt{{x_1}^2 + {y_1}^2}}{\sqrt{{x_2}^2 + {y_2}^2}} e^{i(\delta_1 - \delta_2)}$$

Whereby r_1 and r_2 are absolute values, and $\delta_i = \tan^{-1}\left(\frac{y_i}{x_i}\right)$ for i=1,2 are the phase angles. Applying this representation to the transfer function, the response function becomes,

$$\tilde{u} = \hat{p}\left[\frac{(k^2 + \omega^2 c^2)^{1/2}}{\{\omega^4 m^2 k^2 + (k\omega c - \omega^3 cm)^2\}^{1/2}}\right] e^{i(\delta_1 - \delta_2)} \tag{5.24}$$

Hence, the analytical solution for the frequency-based response amplitude of a spring, mass, damper system in series is given by

$$A(\omega) = \hat{p}\left[\frac{(k^2 + \omega^2 c^2)^{1/2}}{\{\omega^4 m^2 k^2 + (k\omega c - \omega^3 cm)^2\}^{1/2}}\right] \tag{5.25}$$

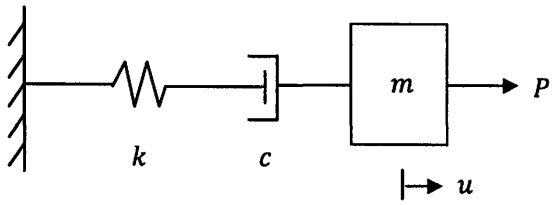

Figure 28: Spring, mass, damper system in series

For an arbitrary system with m = 1000 kg, k = 1000 N/m, and $\hat{p}$ = 1000 N, the response amplitude, A, is plotted as a function of frequency, ω, for different values of damping coefficient, c. The values of c used are [0 400 700 1000 1500 2000 3000 5000 10000] N.s/m, and the resulting plot is shown in Figure 29.

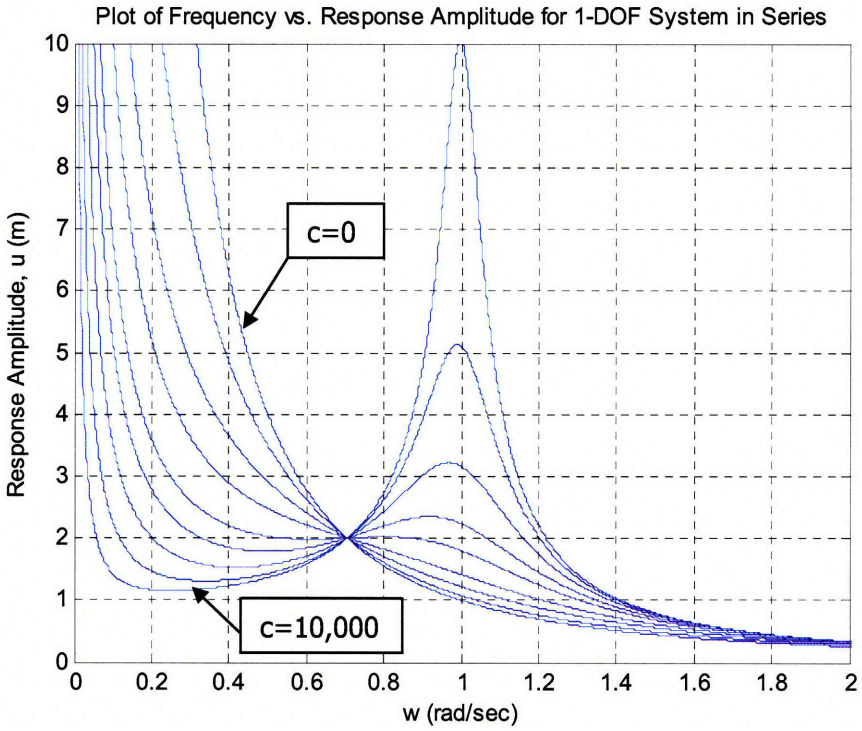

Figure 29: Plot showing variation of response amplitude with frequency

One interesting observation that can be made is that all the curves pass through a common point at $\omega = \sqrt{2}/2$. Mathematically, it can be show that at $\omega = \sqrt{2}/2$, for the given values of k, m, and $\hat{p}$, Equation 5.25 reduces to

$$A(\sqrt{2}/2) = \frac{\sqrt{10^8 + 5 \times 10c^2}}{\sqrt{2.5 \times 10^7 + 1.25 \times 10c^2}} = 2 \times \frac{\sqrt{2.5 \times 10^7 + 1.25 \times 10c^2}}{\sqrt{2.5 \times 10^7 + 1.25 \times 10c^2}} = 2$$

Therefore, the response at this particular frequency is independent of c.

Similar to what is observed in the outrigger system, increasing c initially reduces the response up to a certain point. Increasing c beyond this critical point (for this case ~1500 N.s/m) will yield in an amplification of response around 1 rad/sec, which is the natural frequency of the system corresponding to parallel placement of dampers.

Figure 30 displays pictorially the effect of over-damping in the full scale outrigger model using three different c values (1 low damping value, 1 near the critical level damping, and one over-damped value). The initial reduction in amplitude, response curve passing through a common point at a particular frequency, maximum critical level of damping, and the amplification of response at the shifted frequency are all evident in the plot.

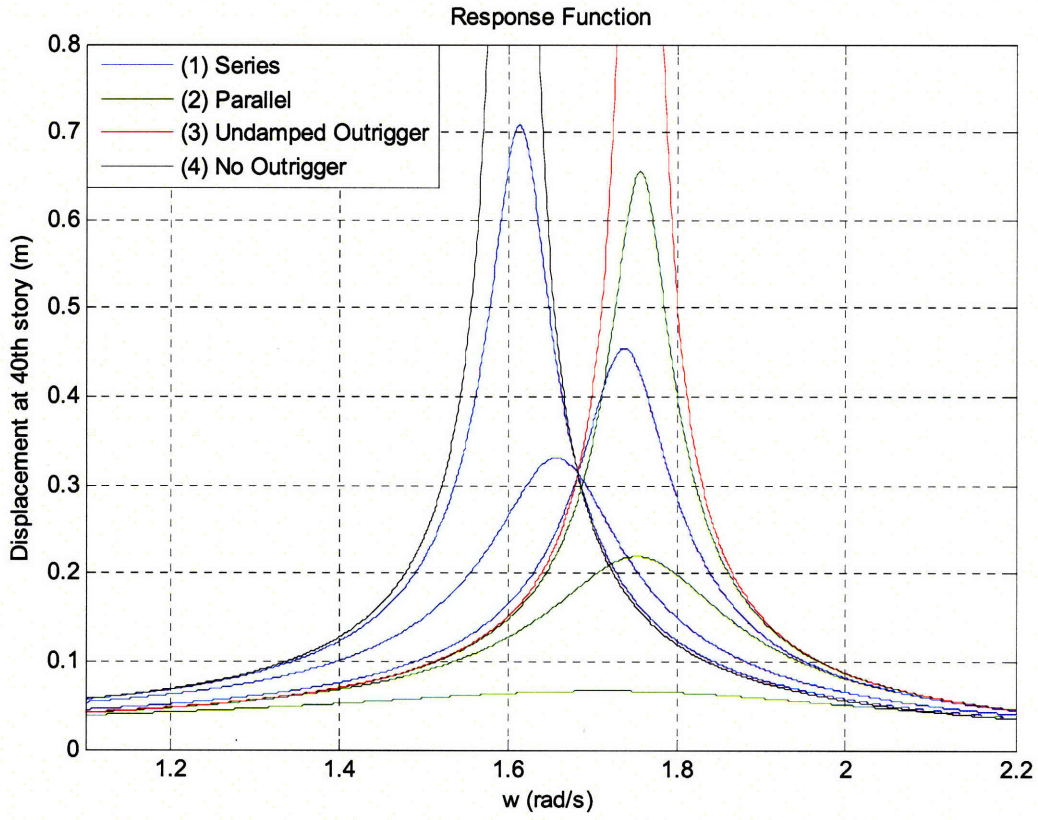

Figure 30: Plot showing effect of over-damping in configuration (1)

5.4.7 Interpretation of Results

The objective in this chapter is to compare configurations (1) - (4) in terms of the performance under static loading, and more importantly the dynamic resonant behavior of the various systems. In section 5.2, the method of incorporating damping effects into the stiffness matrix using the concept of equivalent stiffness is outlined, presenting an elegant way to solve the complex system of matrices.

The benefit of using outriggers is clearly proven under static load, allowing the use of a more economical core design. However, when a damper is placed in series with the perimeter column, the outrigger system does not work under static loading, hence making configuration (1) a less desirable option.

In dynamic analysis, it is shown that damping is achieved more efficiently using configuration (2), i.e. dampers are placed in parallel. The relationship between damping coefficient and overall percent of building damping is linear for configuration (2). This is not the case for configuration (1), whereby a peak effective value exists around 5% critical. Over-damping configuration (1) beyond this point will result in an amplification of response instead. On the other hand, if only a low amount of supplementary damping is desired, configuration (1) provides higher values of percent damping over configuration (2) for a range up to ~3% critical. The difference, however, is not large enough to be a significant benefit.

From the analysis in this chapter, one may conclude that from a structural engineering point of view, configuration (2) performs better compared to configuration (1). It does not sacrifice any static stiffness, and is capable of providing an unrestricted amount of damping as much as space allows.

CHAPTER 6: DESIGN CONSIDERATIONS

6.1 Installation of Damper

The result of dynamic analysis performed in Chapter 5 suggests that viscous dampers should be installed in parallel with the perimeter column where the outrigger connects. However, to achieve this type of parallel connection takes more of a construction challenge than connecting it in line with the column as proposed by Smith and Willford (2007). Two columns side by side will be required to connect the damper in parallel. Alternatively, dampers have to be connected to a rigid floor underneath the outrigger level and possibly back to the column to transfer the loads to the ground. In any case, creating a parallel configuration, although not impossible, will add a significant cost as supposed to making a series connection.

Figure 31 shows a detail of how the damper will be installed at the ends of the outriggers. At this location, the moment in the outrigger arm will be close to zero, hence only shear transfer is required. The two ends of the damper are to be bolted horizontally into the respective connection blocks, transferring shear loads from the outrigger into axial force down the perimeter column. Typically, multiple dampers will be installed at many column locations to spread the damping effect, and add redundancy to the system. This is one of the advantages of using fluid viscous dampers as supposed to using an inertial based damping scheme such as the Tuned Mass Dampers (TMDs) and Tuned Liquid Dampers (TLDs), which focuses all the damping capacity onto one large device.

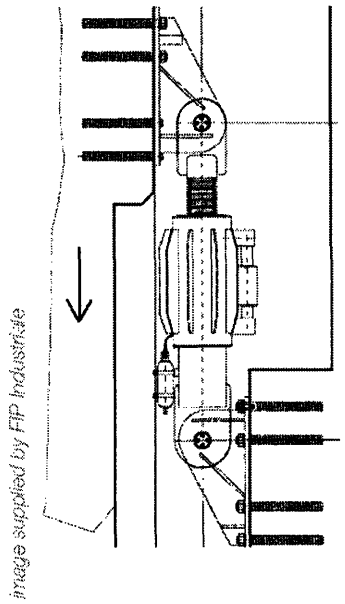

Figure 31: Damper connection detail (Smith & Willford, 2007)

6.2 Moment Connection at Core Wall

Part of the assumptions made during analysis of outrigger system is that the connection between the core and outrigger is rigid. The outrigger itself is also assumed to be rigid and does not bend in double curvature. In actual practice, creating a close to rigid outrigger is best achieved using a truss girder, with the depth of an entire floor in order to provide enough bending stiffness. Using a truss girder instead of a deep plate girder has the advantage of simpler core wall connection as well as a high effective stiffness due to the utilization of axially loaded members. A diagram showing a story deep truss girder connected onto a reinforced concrete core wall is shown in Figure 32.

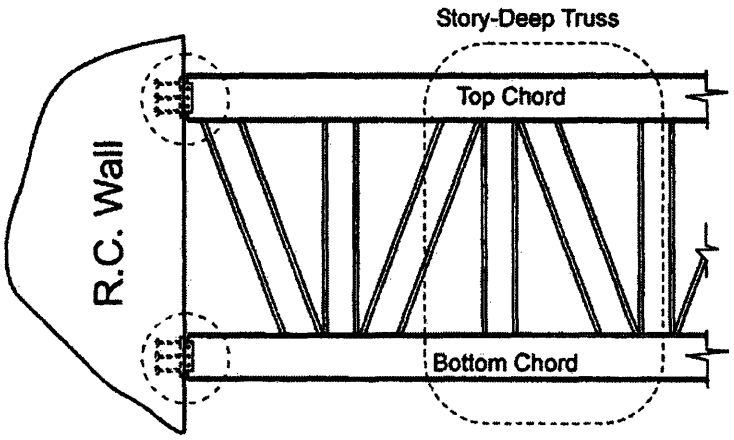

Figure 32: Schematic detail of outrigger truss – core wall connection (Shahrooz, 2004)

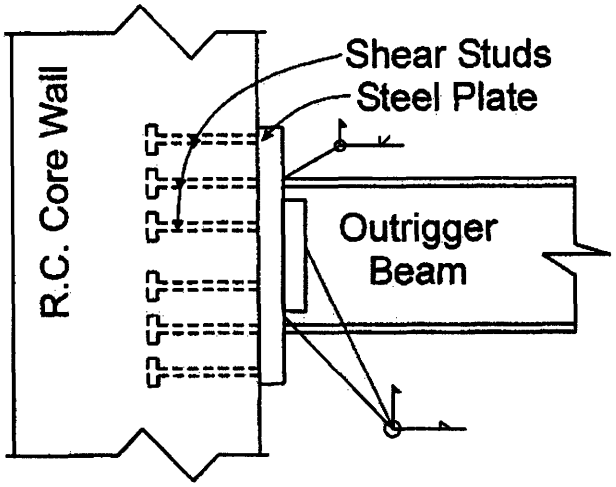

Figure 33: Outrigger beam – core wall moment connection (Shahrooz, 2004)

Connection design is always a major part in every building design, since failures at connections often leads to a brittle collapse. It is always best to ensure that failure occurs in the members itself which has much higher ductility. Figure 33 illustrates a possible moment connection design for the top and bottom chord of the truss girder.

6.3 Finite Element Analysis of Outrigger-Core Wall Connection

In order to prevent connection failure at the core interface, it is important to study how stresses are transferred from the outrigger beam into the reinforced concrete wall through the connection media. The connection detail in Figure 33 will be analyzed in detail using a finite element analysis package ADINA.

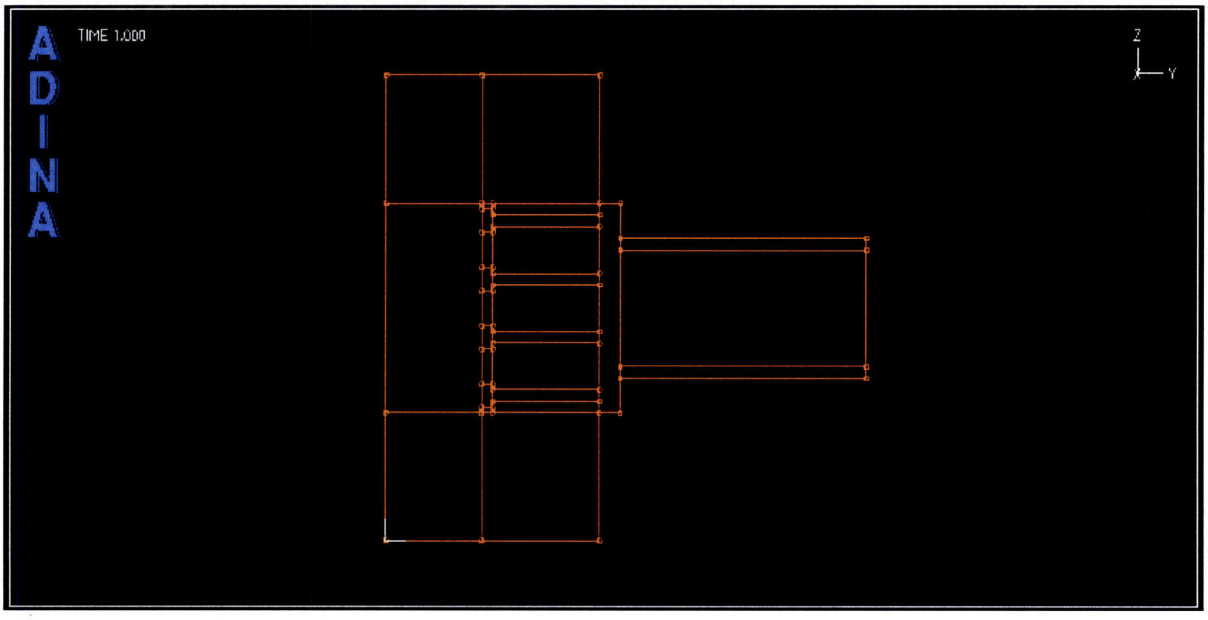

Figure 34: Geometry of outrigger connection as modeled in ADINA

Figure 34 shows the geometry of the outrigger connection as modeled in ADINA. Four shear studs will be used in the analysis. The dimensions used for the different components are summarized in the Table 4. Since the connection will be modeled as a 2-D plane stress analysis, the different components are given a thickness value. The materials are defined as elastic-isotropic, and modulus of elasticity of concrete and steel are taken to be 3600 ksi and 29000 ksi respectively; 0.3 is assumed for the Poisson's ratio in both materials.

Table 4: Dimensions of outrigger connection components (in inches)

Beam	Depth	24
	Flange Thickness	2
	Flange Width	10
	Web Thickness	1
	Section Length	46
Plate	In Plane Thickness	12
	Height	36
	Section Length	4
Studs	Section Length	20
	Cross Section	2x2
Head	Section Length	2
	Cross Section	4x4
Concrete	Length	40
	Height	80
	In Plane Thickness	10

In order to prevent rigid body motion, at least one of the corner points needs to be hinged in the y and z direction. Since a cantilever beam is fixed at the bottom, it is reasonable to model the bottom left corner of the concrete core as a hinge. All other sides are modeled as continuous rollers to allow movement in the y-direction for the top and bottom surface, and z-direction for the side surface.

In order to generate a moment to the shear studs, a unit pressure is applied to the top and bottom flanges in the opposite direction for coupling action. Since this is not a plastic analysis, a unit force is sufficient to give us an understanding of stress distribution around critical elements. Figure 35 shows the connection modeled with a mesh size of 2 by 2 inch, using 9 node elements, and a prescribed pressure at the flanges.

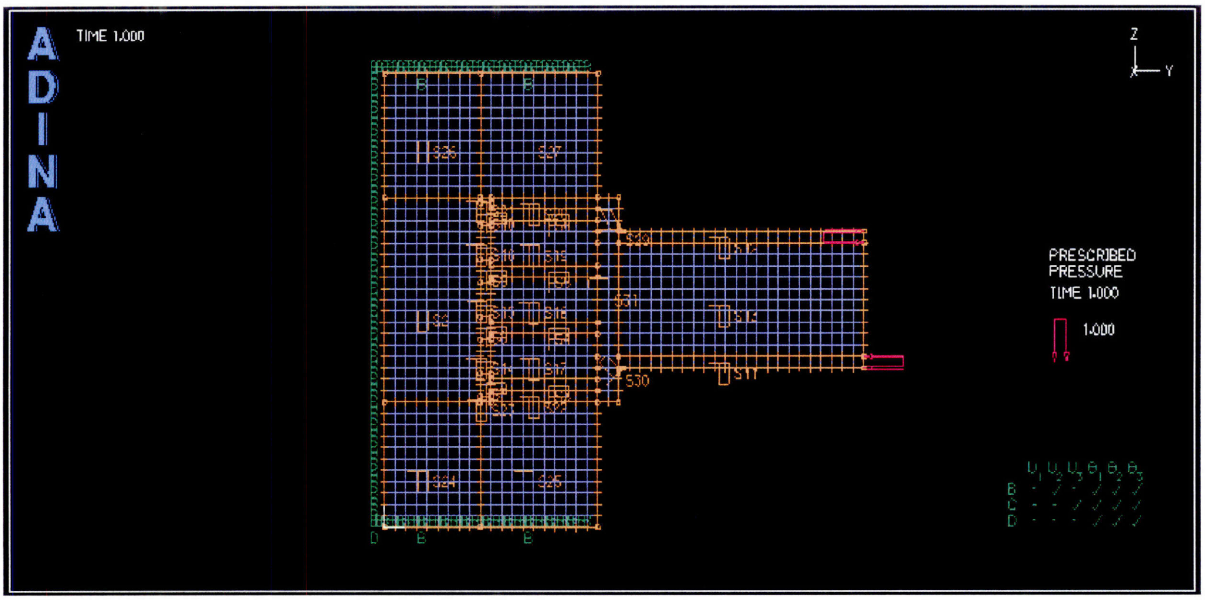

Figure 35: Connection modeled with 2 x 2 mesh, 9 node element, and prescribed pressure

It is found that after several iterations of running the model in ADINA with different element types, and refining the mesh size accordingly, the 9 node element on 2 x 2 inch mesh produces a reasonably accurate result. The effective stress band plot imposed on the deflected shape of the structure is shown in Figure 36.

In the analysis performed, effective stress is shown due to an application of a unit pressure. If actual loads are applied, these stresses will need to be scaled by the corresponding load magnitude. As seen in the Figure 36, the outer shear studs are loaded much severely than the inner ones. It is also observed that the head of the shear studs are effective in shedding stresses gradually into the concrete. The weak point of the system lies primarily in the joint between the stiff plate and the shear studs. Using longer shear studs reduces its stiffness against bending but has a positive effect in transferring stresses deep into the core, away from the stress development near the plate interface.

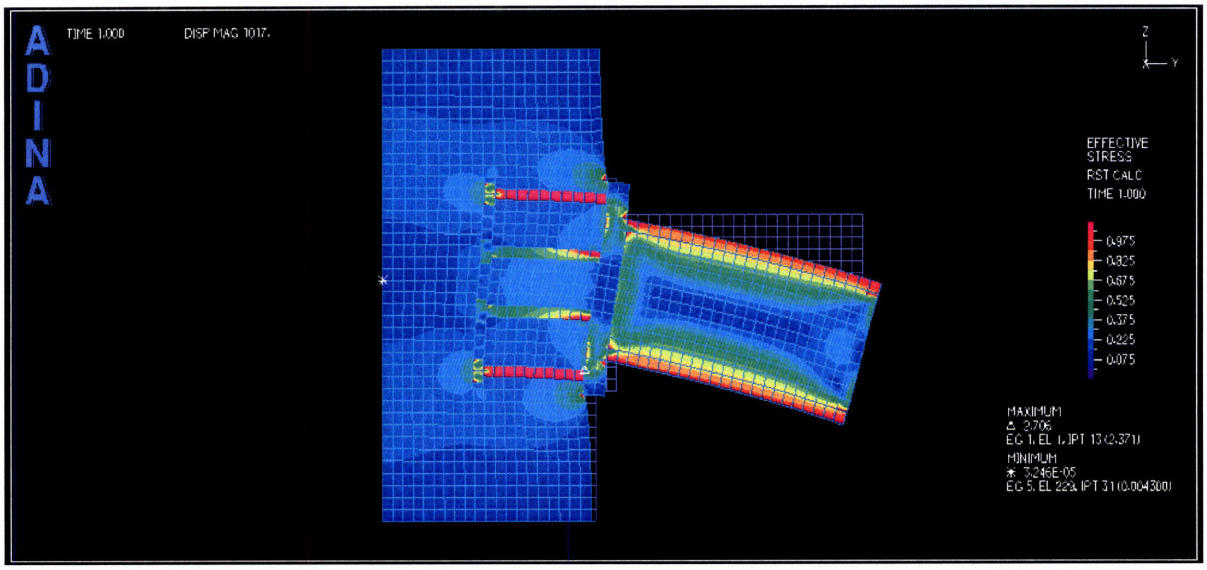

Figure 36: Effective stress band plot imposed on deflected shape

A better way to design the connection is to increase the length of the plate so as to provide better moment transfer. Alternatively, the studs can be reinforced with intermediate grooves to provide better traction into the concrete. As much as possible, studs should be provided away from the bending axis where the moment is largest.

6.4 Other Practical Design Issues

In any damper applications, power dissipation and cooling needs to be considered. The action of dampers results in heat generation in the damping devices. Under the event of an earthquake, the heat generated over 30 seconds can be absorbed safely by the thermal inertia of the units. However, for long duration wind storms, a steady state temperature will be reached, therefore the heat generated must be dissipated safely. The typical amount of heat generated per damper is in the order of 1-3 kW per damper (Smith & Willford, 2007). Passive ventilation from wind can generally be used to cool the dampers.

Viscous dampers generally have a high level of reliability and a spare capacity within the system. Even so, inspection and maintenance is required to ensure long-term performance. The dampers and connections are subjected to millions of cycles of wind-induced vibration over the building's lifetime. It is therefore necessary to check for signs of metal fatigue, cracks, leaks and corrosion. As much as possible, dampers should be protected from the effects of fire and weather elements.

Whenever outriggers are employed, differential shortening between the core and the exterior columns is a common concern particularly in reinforced concrete structures. In the damped outrigger structure, perimeter columns are connected to the outrigger by means of a damper. This means that static differential shortening may occur without generating any force in the outriggers. Thus, the damper stroke needs to be calibrated to account for this settlement.

CHAPTER 7: CONCLUSION

This thesis has shown the effects of incorporating viscous dampers into the outrigger structural system in the design of high-rise buildings. By constructing a discrete lumped mass model and using MATLAB as a simulation tool, a full scale 40-story building has been successfully analyzed with reasonable amount of accuracy. The use of complex stiffness matrix in dynamic analysis eliminates the cost of algebraic computation, leading to a more efficient solution scheme. Two types of damper configurations were studied. Configuration (1) refers to the damper being in series with the perimeter column, and configuration (2) refers to the parallel placement of column and damper. From the frequency-based response functions generated, several conclusions can be made regarding the performance of the two systems.

Configuration (1) is capable of providing a maximum of ~5% supplementary damping at the expense of sacrificing static stiffness. Under this configuration, the core will take the full action of static lateral force since the outriggers do not function when there is no velocity imposed. On the other hand, configuration (2) experience about 17% less deflection under static load due to the rotational stiffness added by the outriggers. Higher levels of supplementary damping can also be achieved with this system, possibly bringing building accelerations under resonance below human comfort limits. There is no effective limit of damping as compared to configuration (1). However, configuration (2) poses more of a construction challenge, and further research has to be done in order to develop a strategy to implement such system with low cost. Unlike configuration (2), configuration (1) can be detailed similar to a regular shear connection, hence easier to construct.

Overall, both configurations (1) and (2) will allow the reduction of member sizes and material due to the reduction of dynamic stiffness required. Viscous dampers can be made highly redundant and reliable, eliminating the need to provide space for devices such as the tuned mass dampers. Damping applies to all frequency range, not only for wind-induced vibrations, but also for seismic excitation. The structural as well as economic benefits of damped outrigger systems have been made clear in this thesis.

REFERENCES

Connor, J. J. (2003). Introduction to Structural Motion Control. New Jersey, NJ: Prentice Hall

Taranath, B. S. (1988). Structural Analysis & Design of Tall Buildings. McGraw Hill, Inc.

Kowalczyk, R. M., Sinn, R. and Kilmister, M. B. (1995). Structural Systems for Tall Buildings. Council on Tall Buildings and Urban Habitat. McGraw Hill, Inc.

Hoenderkamp, J. C. and Bakker, C. M. (2003). Analysis of High-Rise Braced Frames with Outriggers. The Structural Design of Tall and Special Buildings.

Shahrooz, B. M., Deason, J. T. and Tunc, G. (2004). Outrigger Beam – Wall Connections I: Component Testing and Development of Design Model. ASCE Journal of Structural Engineering.

American Society of Civil Engineers/Structural Engineering Institute: Minimum Design Loads for Buildings and Other Structures, 7-05. ASCE Press, 2006.

Smith, R. J. and Willford, M. R. (2007). The Damped Outrigger Concept for Tall Buildings. The Structural Design of Tall and Special Buildings.

Smith, R. J. and Willford, M. R. New Cost-effective Structural Forms for High-Rise Buildings. http://www.arup.com/advancedtechnology/dampingsystems Accessed on May 5, 2008

Irwin, P., RWDI, Inc. Technotes: Architectural/Engineering, Issue No. T02c: Motion Criteria in High Rise Buildings. http://go.rwdi.com/technotes/ Accessed on May 5, 2008

Taylor Devices, Inc. Seismic Dampers and Seismic Protection Products: Seismic Isolation. http://www.taylordevices.com/dampers-seismic-protection.html Accessed on May 5, 2008

APPENDIX A – Calculations of Core & Nodal Properties

Building dimensions:

Building length, $a = 30\ m$

Core length, $b = 14\ m$

Core thickness, $t = 0.4\ m$

Floor height, $c = 4\ m$

Floor thickness, $f = 0.15\ m$

Concrete density, $\rho_c = 2{,}400\ kg/m^3$

Core Properties:

Area of core, $A = b^2 - (b - 2t)^2 = 21.76\ m^2$

Moment of inertia of core, $I = \frac{1}{12}[b^4 - (b - 2t)^4] = 671.37\ m^4$

Floor mass, $m_f = (a^2 - b^2) \times f \times \rho_c = 253{,}440\ kg$

Core mass, $m_c = [b^2 - (b - 2t)^2] \times c \times \rho_c = 208{,}896\ kg$

Nodal Properties:

Nodal Mass, $M = m_f + m_c = 462{,}336\ kg$

Nodal Rotational Inertia,

$J = \frac{1}{12}\{[b^2 \times c \times \rho_c \times (b^2 + c^2)] - \{(b - 2t)^2 \times c \times \rho_c \times [(b - 2t)^2 + c^2]\}\} = 6{,}723{,}666\ kgm^2$

APPENDIX B – MATLAB Code for Static Analysis

```
% Outrigger Static Analysis Program

clear all
close all
clc

% Core Properties

A = 21.76; % Area of Core (m^2)
E = 2.482e10; % Young's Modulus (Pa)
I = 671; % Moment of Inertia (m^4)
L = 4; % Story Height (m)
a = 0; % Rotation angle, rad
F = 323753; % Applied Load at Nodes (N)

% Outrigger Properties

Story = 21; % Location of Outrigger (Story 1-40)
xr = Story*2; % Matrix Location Rotational Spring Index
b = 8; % Outrigger Length (m)
Acol = 0.15; % Area of Column (m^2)
Ecol = 2e11; % Column Young's Modulus (Pa)
Lcol = Story*L; % Length of Column (m)
c = 100000000; % Damper Coefficient (N.s/m)

% Stiffness Definition

w = 0; % frequency set to zero for static analysis

Kcol = Acol*Ecol/Lcol; % Stiffness of Column (N/m)
Keq1 = (Kcol*i*w*c)/(i*w*c+Kcol); % Series
Keq2 = i*w*c+Kcol; % Parallel
Keq3 = Kcol; % No Damper
Kr1 = 2*b^2*Keq1; % Outrigger Rotational Stiffness - Series
Kr2 = 2*b^2*Keq2; % Outrigger Rotational Stiffness - Parallel
Kr3 = 2*b^2*Keq3; % Outrigger Rotational Stiffness - No Damper

% Generate Stiffness Matrix, Load Vector and Displacement Vector

[K1,P1,u1,U1,x1,y1] = discrete40_static(A,E,I,L,a,F,xr,Kr1);
[K2,P2,u2,U2,x2,y2] = discrete40_static(A,E,I,L,a,F,xr,Kr2);
[K3,P3,u3,U3,x3,y3] = discrete40_static(A,E,I,L,a,F,xr,Kr3);
[K4,P4,u4,U4,x4,y4] = discrete40_static_norig(A,E,I,L,a,F);
```

```
utop1 = U1(79); % Maximum Top Deflection for Configuration 1
utop2 = U2(79); % Maximum Top Deflection for Configuration 2
utop3 = U3(79); % Maximum Top Deflection for Configuration 3
utop4 = U4(79); % Maximum Top Deflection for Configuration 4

% Plot Displacement Profile

figure(1)
plot(x1,y1,'*',x2,y2,'o',x3,y3,'.-',x4,y4,'k-')
title('Displacement Profile Under Static Load')
xlabel('Horizontal Displacement (m)')
ylabel('Height (m)')
legend('(1) Series','(2) Parallel','(3) Undamped Outrigger','(4) No
Outrigger')
axis auto
grid on


function [K,P,u,U,x,y] = discrete40_static(A,E,I,L,a,F,xr,Kr)

Kaa = [A*E/L*(sin(a))^2 + (12*E*I)/(L^3)*(cos(a))^2, 6*E*I/(L^2)*cos(a);
       6*E*I/(L^2)*cos(a), 4*E*I/L];
Kab = [-(A*E/L*(sin(a))^2 + (12*E*I)/(L^3)*(cos(a))^2), 6*E*I/(L^2)*cos(a);
       -6*E*I/(L^2)*cos(a), 2*E*I/L];
Kba = [-(A*E/L*(sin(a))^2 + (12*E*I)/(L^3)*(cos(a))^2), -6*E*I/(L^2)*cos(a);
       6*E*I/(L^2)*cos(a), 2*E*I/L];
Kbb = [A*E/L*(sin(a))^2 + (12*E*I)/(L^3)*(cos(a))^2, -6*E*I/(L^2)*cos(a);
       -6*E*I/(L^2)*cos(a), 4*E*I/L];

k = [Kaa Kab; Kba Kbb];
kmid = [k(1:2,1:2) + k(3:4,3:4)];

for i=1:2:77
    K(i:i+3,i:i+3) = k;
end
for i=1:2:77
    K(i:i+1,i:i+1) = kmid;
end

K(xr,xr) = K(xr,xr) + Kr;

P = zeros(80,1);
P(1:2:79) = F;

u = K\P;

U = (real(u).^2 + imag(u).^2).^(0.5);

x(2:41) = U(1:2:79);
y(2:41) = [4:4:160];
```

```
function [K,P,u,U,x,y] = discrete40_static_norig(A,E,I,L,a,F)

Kaa = [A*E/L*(sin(a))^2 + (12*E*I)/(L^3)*(cos(a))^2, 6*E*I/(L^2)*cos(a);
       6*E*I/(L^2)*cos(a), 4*E*I/L];
Kab = [-(A*E/L*(sin(a))^2 + (12*E*I)/(L^3)*(cos(a))^2), 6*E*I/(L^2)*cos(a);
       -6*E*I/(L^2)*cos(a), 2*E*I/L];
Kba = [-(A*E/L*(sin(a))^2 + (12*E*I)/(L^3)*(cos(a))^2), -6*E*I/(L^2)*cos(a);
       6*E*I/(L^2)*cos(a), 2*E*I/L];
Kbb = [A*E/L*(sin(a))^2 + (12*E*I)/(L^3)*(cos(a))^2, -6*E*I/(L^2)*cos(a);
       -6*E*I/(L^2)*cos(a), 4*E*I/L];

k = [Kaa Kab; Kba Kbb];
kmid = [k(1:2,1:2) + k(3:4,3:4)];

for i=1:2:77
    K(i:i+3,i:i+3) = k;
end
for i=1:2:77
    K(i:i+1,i:i+1) = kmid;
end

P = zeros(80,1);
P(1:2:79) = F;

u = K\P;

U = (real(u).^2 + imag(u).^2).^(0.5);

x(2:41) = U(1:2:79);
y(2:41) = [4:4:160];
```

APPENDIX C – MATLAB Code for Dynamic Analysis

```
% Outrigger Dynamic Analysis Program

clear all
close all
clc

% Core Properties

A = 21.76; % Area of Core (m^2)
E = 2.482e10; % Young's Modulus (Pa)
I = 671; % Moment of Inertia (m^4)
L = 4; % Story Height (m)
a = 0; % Rotation angle, rad
F = 23800; % Applied Load at nodes (N)

% Outrigger Properties

Story = 21; % Location of Outrigger (Story 1-40)
xr = Story*2; % Matrix Location Rotational Spring Index
b = 8; % Outrigger Length (m)
Acol = 0.15; % Area of Column (m^2)
Ecol = 2e11; % Column Young's Modulus (Pa)
Lcol = Story*L; % Length of Column (m)

% ANALYSIS 1 - MODAL ANALYSIS

% Stiffness Definition

w = 0; % Frequency Set to zero for Modal Analysis
c = 0; % Damper Coefficient (N.s/m)

Kcol = Acol*Ecol/Lcol; % Stiffness of Column (N/m)
Keq1 = (Kcol*i*w*c)/(i*w*c+Kcol); % Series
Keq2 = i*w*c+Kcol; % Parallel
Keq3 = Kcol; % No Damper
Kr1 = 2*b^2*Keq1; % Outrigger Rotational Stiffness - Series
Kr2 = 2*b^2*Keq2; % Outrigger Rotational Stiffness - Parallel
Kr3 = 2*b^2*Keq3; % Outrigger Rotational Stiffness - No Damper

% Generate Mass Matrix, Stiffness Matrix, Load Vector and Displacement Vector

[M1,K1,P1,Co1,u1,U1,x1,y1] = discrete40_dynamic(A,E,I,L,a,F,xr,Kr1,w);
[M2,K2,P2,Co2,u2,U2,x2,y2] = discrete40_dynamic(A,E,I,L,a,F,xr,Kr2,w);
[M3,K3,P3,Co3,u3,U3,x3,y3] = discrete40_dynamic(A,E,I,L,a,F,xr,Kr3,w);
[M4,K4,P4,Co4,u4,U4,x4,y4] = discrete40_dynamic_norig(A,E,I,L,a,F,w);
```

```
% Generate Eigenvalues

[X1,L1] = eig(K1,M1);
[X2,L2] = eig(K2,M2);

% Frequency

ev1 = diag(L1);
ev2 = diag(L2);

omega1_1 = ev1(1)^(0.5)
omega2_1 = ev2(1)^(0.5)
omega1_2 = ev1(2)^(0.5)
omega2_2 = ev2(2)^(0.5)
omega1_3 = ev1(3)^(0.5)
omega2_3 = ev2(3)^(0.5)

% Period

period1_1 = 2*pi/omega1_1
period2_1 = 2*pi/omega2_1
period1_2 = 2*pi/omega1_2
period2_2 = 2*pi/omega2_2
period1_3 = 2*pi/omega1_3
period2_3 = 2*pi/omega2_3

% Mode Shapes (Series)

col1 = X1(:,1);
mode1(2:41) = col1(1:2:79);
figure(1)
subplot(1,3,1)
plot(mode1,y1,'-*')
title('First Mode')
ylabel('Height (m)')
grid on

col2 = X1(:,2);
mode2(2:41) = col2(1:2:79);
subplot(1,3,2)
plot(mode2,y1,'-*')
title('Second Mode')
ylabel('Height (m)')
grid on

col3 = X1(:,3);
mode3(2:41) = col3(1:2:79);
subplot(1,3,3)
plot(mode3,y1,'-*')
title('Third Mode')
ylabel('Height (m)')
grid on
```

```
% Mode Shapes (Parallel)

col1 = X2(:,1);
mode1(2:41) = col1(1:2:79);
figure(2)
subplot(1,3,1)
plot(mode1,y1,'-*')
title('First Mode')
ylabel('Height (m)')
grid on

col2 = X2(:,2);
mode2(2:41) = col2(1:2:79);
subplot(1,3,2)
plot(mode2,y1,'-*')
title('Second Mode')
ylabel('Height (m)')
grid on

col3 = X2(:,3);
mode3(2:41) = col3(1:2:79);
subplot(1,3,3)
plot(mode3,y1,'-*')
title('Third Mode')
ylabel('Height (m)')
grid on

% ANALYSIS 2 - Frequency-Based Response for First, Second and Third Mode

z = 1;

for w = 1:0.01:30 % Frequency of Excitation

% Stiffness Definition

c = 100000000; % Damper Coefficient (N.s/m)

Kcol = Acol*Ecol/Lcol; % Stiffness of Column (N/m)
Keq1 = (Kcol*i*w*c)/(i*w*c+Kcol); % Series
Keq2 = i*w*c+Kcol; % Parallel
Keq3 = Kcol; % No Damper
Kr1 = 2*b^2*Keq1; % Outrigger Rotational Stiffness - Series
Kr2 = 2*b^2*Keq2; % Outrigger Rotational Stiffness - Parallel
Kr3 = 2*b^2*Keq3; % Outrigger Rotational Stiffness - No Damper

% Generate Mass Matrix, Stiffness Matrix, Load Vector and Displacement Vector

[M1,K1,P1,Co1,u1,U1,x1,y1] = discrete40_dynamic(A,E,I,L,a,F,xr,Kr1,w);
[M2,K2,P2,Co2,u2,U2,x2,y2] = discrete40_dynamic(A,E,I,L,a,F,xr,Kr2,w);
[M3,K3,P3,Co3,u3,U3,x3,y3] = discrete40_dynamic(A,E,I,L,a,F,xr,Kr3,w);
[M4,K4,P4,Co4,u4,U4,x4,y4] = discrete40_dynamic_norig(A,E,I,L,a,F,w);
```

```
utop1(z) = U1(79); % Horizontal Deflection at Top for Configuration 1
utop2(z) = U2(79); % Horizontal Deflection at Top for Configuration 2
utop3(z) = U3(79); % Horizontal Deflection at Top for Configuration 3
utop4(z) = U4(79); % Horizontal Deflection at Top for Configuration 4

z = z + 1;

end

% Plot Response Curves

figure (3)
w = 1:0.01:30;
plot(w,utop1,w,utop2,w,utop3,w,utop4,'k')
title('Frequency-Based Response Function')
xlabel('w (rad/s)')
legend('(1) Series','(2) Parallel','(3) Undamped Outrigger','(4) No
Outrigger')
ylabel('Displacement at 40th story (m)')
axis([1 30 0 0.5])
grid on

figure (4)
T = 2.*pi./w;
plot(T,utop1,T,utop2,T,utop3,T,utop4,'k')
title('Period-Based Response Function')
xlabel('T (seconds)')
legend('(1) Series','(2) Parallel','(3) Undamped Outrigger','(4) No
Outrigger')
ylabel('Displacement at 40th story (m)')
axis([0 5 0 0.5])
grid on

% ANALYSIS 3 - Resonance at Fundamental Period

for C = [50000000 150000000 500000000]

z = 1;

for w = 1.1:0.001:2.2 % Frequency of Excitation

% Stiffness Definition

c = C; % Damper Coefficient (N.s/m)

Kcol = Acol*Ecol/Lcol; % Stiffness of Column (N/m)
Keq1 = (Kcol*i*w*c)/(i*w*c+Kcol); % Series
Keq2 = i*w*c+Kcol; % Parallel
Keq3 = Kcol; % No Damper
Kr1 = 2*b^2*Keq1; % Outrigger Rotational Stiffness - Series
Kr2 = 2*b^2*Keq2; % Outrigger Rotational Stiffness - Parallel
Kr3 = 2*b^2*Keq3; % Outrigger Rotational Stiffness - No Damper
```

```
% Generate Mass Matrix, Stiffness Matrix, Load Vector and Displacement Vector

[M1,K1,P1,Co1,u1,U1,x1,y1] = discrete40_dynamic(A,E,I,L,a,F,xr,Kr1,w);
[M2,K2,P2,Co2,u2,U2,x2,y2] = discrete40_dynamic(A,E,I,L,a,F,xr,Kr2,w);
[M3,K3,P3,Co3,u3,U3,x3,y3] = discrete40_dynamic(A,E,I,L,a,F,xr,Kr3,w);
[M4,K4,P4,Co4,u4,U4,x4,y4] = discrete40_dynamic_norig(A,E,I,L,a,F,w);

ut1(z) = U1(79); % Horizontal Deflection Magnitude at Top for Configuration 1
ut2(z) = U2(79); % Horizontal Deflection Magnitude at Top for Configuration 2
ut3(z) = U3(79); % Horizontal Deflection Magnitude at Top for Configuration 3
ut4(z) = U4(79); % Horizontal Deflection Magnitude at Top for Configuration 4

z = z + 1;

end

% Plot Response Curves

figure (5)
w = 1.1:0.001:2.2;
plot(w,ut1,w,ut2,w,ut3,w,ut4,'k')
title('Response Function')
xlabel('w (rad/s)')
legend('(1) Series','(2) Parallel','(3) Undamped Outrigger','(4) No
Outrigger')
ylabel('Displacement at 40th story (m)')
axis([1.1 2.2 0 0.8])
grid on
hold on

end

% Building Acceleration at Fundamental Mode Resonance

maxaccel1 = max(ut1)*omega1_1^2
maxaccel2 = max(ut2)*omega2_1^2

% Half Power Bandwidth Method

% Series

Amax1 = max(ut1);
Ahalf1 = Amax1/(2^(0.5));
ut1_scaled = ut1 - Ahalf1;
Array1 = (ut1_scaled > 0);
```

```
for q=1:length(w)
    if Array1(q) == 1
        loc1_1 = q;
        break
    end
end
for r=loc1_1:length(w)
    if Array1(r) == 0
        loc2_1 = r;
        break
    end
end

w1_1 = w(loc1_1);
w2_1 = w(loc2_1);

% Parallel

Amax2 = max(ut2);
Ahalf2 = Amax2/(2^(0.5));
ut2_scaled = ut2 - Ahalf2;
Array2 = (ut2_scaled > 0);

for q=1:length(w)
    if Array2(q) == 1
        loc1_2 = q;
        break
    end
end
for r=loc1_2:length(w)
    if Array2(r) == 0
        loc2_2 = r;
        break
    end
end

w1_2 = w(loc1_2);
w2_2 = w(loc2_2);

% Estimate % Damping

ksi_series = (w2_1 - w1_1)/(w2_1 + w1_1)
ksi_parallel = (w2_2 - w1_2)/(w2_2 + w1_2)
```

```
function [M,K,P,Co,u,U,x,y] = discrete40_dynamic(A,E,I,L,a,F,xr,Kr,w)

Kaa = [A*E/L*(sin(a))^2 + (12*E*I)/(L^3)*(cos(a))^2, 6*E*I/(L^2)*cos(a);
       6*E*I/(L^2)*cos(a), 4*E*I/L];
Kab = [-(A*E/L*(sin(a))^2 + (12*E*I)/(L^3)*(cos(a))^2), 6*E*I/(L^2)*cos(a);
       -6*E*I/(L^2)*cos(a), 2*E*I/L];
Kba = [-(A*E/L*(sin(a))^2 + (12*E*I)/(L^3)*(cos(a))^2), -6*E*I/(L^2)*cos(a);
       6*E*I/(L^2)*cos(a), 2*E*I/L];
Kbb = [A*E/L*(sin(a))^2 + (12*E*I)/(L^3)*(cos(a))^2, -6*E*I/(L^2)*cos(a);
       -6*E*I/(L^2)*cos(a), 4*E*I/L];

k = [Kaa Kab; Kba Kbb];
kmid = [k(1:2,1:2) + k(3:4,3:4)];

for i=1:2:77
    K(i:i+3,i:i+3) = k;
end
for i=1:2:77
    K(i:i+1,i:i+1) = kmid;
end

K(xr,xr) = K(xr,xr) + Kr;

Z = [462336 0; 0 6723666];
M =
blkdiag(Z,Z,Z,Z,Z,Z,Z,Z,Z,Z,Z,Z,Z,Z,Z,Z,Z,Z,Z,Z,Z,Z,Z,Z,Z,Z,Z,Z,Z,Z,Z,Z,Z,Z,Z
,Z,Z,Z,Z,Z);

P = zeros(80,1);
P(1:2:79) = F;

Co = K - (w^2).*M;

u = Co\P;

U = (real(u).^2 + imag(u).^2).^(0.5);

x(2:41) = U(1:2:79);
y(2:41) = [4:4:160];
```

```
function [M,K,P,Co,u,U,x,y] = discrete40_dynamic_norig(A,E,I,L,a,F,w)

Kaa = [A*E/L*(sin(a))^2 + (12*E*I)/(L^3)*(cos(a))^2, 6*E*I/(L^2)*cos(a);
       6*E*I/(L^2)*cos(a), 4*E*I/L];
Kab = [-(A*E/L*(sin(a))^2 + (12*E*I)/(L^3)*(cos(a))^2), 6*E*I/(L^2)*cos(a);
       -6*E*I/(L^2)*cos(a), 2*E*I/L];
Kba = [-(A*E/L*(sin(a))^2 + (12*E*I)/(L^3)*(cos(a))^2), -6*E*I/(L^2)*cos(a);
       6*E*I/(L^2)*cos(a), 2*E*I/L];
Kbb = [A*E/L*(sin(a))^2 + (12*E*I)/(L^3)*(cos(a))^2, -6*E*I/(L^2)*cos(a);
       -6*E*I/(L^2)*cos(a), 4*E*I/L];

k = [Kaa Kab; Kba Kbb];
kmid = [k(1:2,1:2) + k(3:4,3:4)];

for i=1:2:77
    K(i:i+3,i:i+3) = k;
end
for i=1:2:77
    K(i:i+1,i:i+1) = kmid;
end

Z = [462336 0; 0 6723666];
M =
blkdiag(Z,Z,Z,Z,Z,Z,Z,Z,Z,Z,Z,Z,Z,Z,Z,Z,Z,Z,Z,Z,Z,Z,Z,Z,Z,Z,Z,Z,Z,Z,Z,Z,Z,Z,Z
,Z,Z,Z,Z,Z);

P = zeros(80,1);
P(1:2:79) = F;

Co = K - (w^2).*M;

u = Co\P;

U = (real(u).^2 + imag(u).^2).^(0.5);

x(2:41) = U(1:2:79);
```

APPENDIX D – Other MATLAB Codes

```
% Single Outrigger Analytical Solution

b = 8; % m
A = 0.15; % m^2
P = 323753; % N
H = 160; % m
n = 40; % # floors
w = n*P/H; % N/m
Ecol = 2e11; % Pa
E = 2.482e10; % Pa
I = 671; % m^4

a1 = ((9*b^2*A*Ecol+3*I*E)+(57*b^4*A^2*Ecol^2+36*I*b^2*A*Ecol*E-
9*E^2)^(0.5))/(4*b^2*A*Ecol+3*I*E)
a2 = ((9*b^2*A*Ecol+3*I*E)-(57*b^4*A^2*Ecol^2+36*I*b^2*A*Ecol*E-
9*E^2)^(0.5))/(4*b^2*A*Ecol+3*I*E)

a = 0.5265;

f = (1-a+a^2/3)/(1+E*I/(2*b^2*A*Ecol));

uh = (w*H^4)/(8*E*I)
uh_out = (w*H^4)/(8*E*I)*(1-f*(4*a*(1-a)+2*a^2))


% Plot c vs. ksi

c = [10000 50000 80000 90000 100000 150000 200000 250000 300000 350000 400000
450000 500000];
s = [0.0044 0.0217 0.0320 0.0350 0.0377 0.0456 0.0471 0.0451 0.0418 0.0383
0.0350 0.0320 0.0293].*100;
p = [0.0040 0.0196 0.0316 0.0353 0.0393 0.0594 0.0799 0.1004 0.1220 0.1445
0.1681 0.1929 0.2193].*100;

plot(c,s,'-',c,p,'r:')
title('Plot of Damping Coefficient vs. % Critical Damping')
xlabel('c (kN.s/m)')
ylabel('% critical damping')
legend('Series','Parallel')
grid on
```